博士論文

Catalytic Mechanism of Transition Metal Oxides for Hydrogen Absorption and Desorption Reactions of Magnesium

マグネシウムの水素吸蔵／放
出反応における遷移金属酸化
物の触媒機構

木 村 通

広島大学大学院先端物質科学研究科

2014 年 3 月

目次

主論文

Abstract

Magnesium (Mg) is recognized as one of the attractive materials for hydrogen storage because it can store 7.6 mass% of hydrogen and is relatively abundant element. However, the surface is not active for dissociation/recombination of hydrogen molecules, resulting in the reaction rates for hydrogen absorption and desorption reactions are very slow. It suggests that the energy barrier, which is generally called the activation energy, for dissociation and recombine of hydrogen molecular bonding is large. Actually, heat activation is required for the hydrogen absorption of pure Mg in despite of the reaction is exothermic. So far, ball milling and addition of catalysts have been used as techniques of decreasing the activation energy. Transition metal oxides have been reported as better catalysts for the Mg-H system than typical transition metal catalysts such as Ni. Among them, niobium (Nb) oxide shows a remarkable catalytic effect. In general, the catalytic effect of transition metals is understood as follows: transition metals have d-electrons which are spatially-distributed widely, and the electrons interact with the non-bonding orbital of hydrogen molecules, thereby the activation energy for dissociation of hydrogen molecules is reduced. And then, the dissociated hydrogen atoms diffuse on the surface of catalysts. On the other side, the catalytic mechanism of transition metal oxides have never been revealed, and it is probably not the same as the above typical metal catalysts.

The purpose of this thesis is to investigate the catalytic effects of Nb_2O_5 for hydrogen absorption and desorption of Mg, and the rate-determining step and catalytic mechanism are discussed.

In the hydrogen desorption reaction, the activation energy (E_{des}) of MgH_2 with

and without Nb_2O_5 were estimated as 70 and 127 kJ/mol, respectively, indicating that the addition of Nb_2O_5 activated the surface of MgH_2. And the value of MgH_2 with Nb_2O_5, 70 kJ/mol, was almost same as the enthalpy change (ΔH) from MgH_2 to Mg, 74 kJ/mol. On the hydrogen absorption, a drastic improvement of kinetics was found. The reaction can be proceeded even under −50 °C with 0.2 MPa of H_2. The activation energy for hydrogen absorption reaction of Mg (E_{abs}) with and without Nb_2O_5 were estimated as 38 and 61 kJ/mol, respectively. According to the above results, the kinetics of reactions between Mg and H_2 is considered as below. For pure Mg, the energy barrier caused by dissociation and recombination of H_2 on the Mg surface is largest in the reaction process. Thus, the 61 kJ/mol of extra energy is required to realize the H_2 absorption, and it was observed as E_{abs}. For the H_2 desorption reaction, it is expected that the total energy, which includes the activation energy E_{abs} and enthalpy change ΔH, is observed as E_{des}. In fact, the E_{des} value obtained by the experiments was 129 kJ/mol, which is close to the expected value ($E_{abs} + \Delta H = 61 + 74 = 135$ kJ/mol). On the other hand, the E_{des} of Mg catalyzed with Nb_2O_5 was thought to be corresponding to ΔH because the energy barrier was drastically reduced by the catalyst. For the absorption reaction, the rate-determining step should be changed from H_2 dissociation on the surface to another reaction. E_{abs} was estimated as 38 kJ/mol, and the value was close to 40 kJ/mol reported as the activation energy for hydrogen diffusion in Mg.

The chemical states of Nb added in Mg as the catalyst have been investigated by X-ray absorption spectroscopy (XAS). It was reported that its chemical state was changed to NbO because both spectra of X-ray absorption near edge structure (XANES) of Nb K-edge were almost same. In this study, the variation on the chemical state of Nb in hydrogen absorption and desorption process was *in-situ* investigated by energy

dispersive X-ray absorption fine structure (DXAFS) at the synchrotron radiation facility (SPring-8, Japan). For the *in-situ* condition, an original reaction cell was made to utilize hydrogen in SPring-8. The XANES spectrum was gradually shifted up to high energy during the hydrogenation. The energy shift was much smaller than the shift derived from valence variation such as Nb $\leftrightarrow$ Nb$_2$O$_5$, suggesting that the observed spectral change is not originated in the valence variation. The radial distribution function around Nb atom was obtained by analysis of the extended X-ray absorption fine structure (EXAFS). On the hydrogen absorption reaction, the intensity of the second nearest atoms, which were neighbor Nb atoms, was decreasing without the shift of peak position by the hydrogenation. This result would suggest that hydrogen atoms passed through highly dispersed Nb catalysts with nano size, and they were further became small during the hydrogenation. The small variation of XANES spectra would be caused by the decrease in the crystalline size of Nb catalysts. For the hydrogen desorption reaction, a continuous change shown in hydrogen absorption was not observed. It indicated that the two effects, which were crystalline growth by heating and crystalline reduce by passing of hydrogen atoms, competed with each other. In fact, by comparison of results before and after dehydrogenation under room temperature condition, the Nb crystalline was grown by heating during hydrogen desorption process. On the basis of these results, the reaction process between Mg catalyzed Nb$_2$O$_5$ and hydrogen is proposed as bellow. Regarding the hydrogen absorption process, hydrogen molecules are dissociated to H atoms on Nb oxide catalyst. The dissociated atoms diffuse to inside of the catalyst and are rapidly transferred to Mg. And then, the crystalline size of the catalyst was reduced by the diffusion effects. For the hydrogen desorption process, the crystalline size of Nb oxide is not changed during hydrogen desorption reaction because of competition between the

effects of heating and H diffusion, however it is grown up after finished the reaction.

In conclusion of this study, the catalyst effect of Nb_2O_5 for hydrogen absorption and desorption of Mg decreases the energy barrier for dissociation and recombination of hydrogen molecules, and as the result, the rate-determining step of hydrogen absorption reaction of Mg is changed. Besides, when hydrogen atoms pass to Mg, the atoms diffuse not on the catalyst surface as conventional transition metal catalysts but through its inside part.

Acknowledgements

Contents

1   Introduction

1.1   Hydrogen energy

Since the "Industrial Revolution", we have continued the drastic development with consumption of the fossil fuels all over the world. The energy consumption is still increasing to develop our comfortable lives, and the main fuels have been changed from coal to oil and natural gas. However, the depletion of oil has been feared within several decades. In addition, the fossil fuels are concerned to cause environmental damage because carbon dioxide, nitrogen oxide, and sulfur dioxide have been generated during the energy utilization by combustion of them. Therefore, the novel energy system except for the utilization of the above fossil fuels is needed to be explored. Ideally, the alternate primary energy is the natural energy such as solar, wind, geothermal, and hydro energy. The natural energy is totally renewable and suitable to establish the sustainable society, however there are three big problems as follows.

i. Some energy resources, especially solar energy and wind energy, fluctuates with time cycle of the earth.

ii. Energy resources are localized to limited areas.

iii. Huge area to collect and utilize natural energy is required because of the dilute energy density.

Thus, the efficient conversion techniques from natural energy to secondary energy such as electricity and hydrogen are necessary to store and distribute the energy. So far, the power generation techniques, which convert the natural energy to electricity,

have been well achieved with high efficiency. Regarding the solar power utilization, above 44 % efficiency could be achieved by using concentration technique of solar light in recent years [1]. However, electric energy is unsuitable to store and transport the large amount of energy.

Hydrogen is attractive for the energy storage and transportation because it has higher gravimetric energy density, which is about 120 kJ/g by combustion [2], than fossil fuels. Moreover, the environmental load on the utilization of hydrogen is very low, because the water is only generated as a product after combustion. In addition, hydrogen can be generated from water by various kinds of methods. From the above points, hydrogen is recognized as the most prospective secondary energy. However, the volumetric energy density is extremely low because hydrogen is gaseous phase under ambient condition. Thus, the storage technology in the compact size is required for the storage and transportation of a massive energy.

1.2   Hydrogen storage

As the hydrogen storage technique, a various methods have been researched at present. The typical methods among them are described as follows.

1.2.1 Compressed hydrogen

The compressed hydrogen is the simplest method for hydrogen storage, and the hydrogen is stored by using high-pressure cylinder. By development of the cylinder material to withstand the higher pressure, the capacity of hydrogen storage has been improved. In recent years, the cylinder has been able to store 70 MPa of H_2 by using aluminum alloy and carbon fiber, suggesting that the hydrogen density has reached up

to 39 kg/m^3, and the cylinder would be suitable for on-board application because of quick hydrogen filling and release [2, 3]. Actually, the high-pressure cylinder is used for fuel tank of FCV (fuel cell vehicle), which has succeeded in driving more than 800 km without hydrogen refilling [3]. However, all the problems such as size, cost, and safety, have not been solved yet.

1.2.2 Liquid hydrogen

The volumetric density of liquid hydrogen, 71 kg/m^3 at -253 °C, is more than 800 times larger than that of gaseous state, 0.81 kg/m^3 at 25 °C under 0.1 MPa [2], which is one of solutions to the problem of low volumetric energy density. This technique has been developed as a rocket's propulsion fuel, and today, it is especially used for the massive storage and transportation of commercial hydrogen. However, a large energy is required for the liquefaction because its boiling point under atmospheric pressure is about 20 K. Moreover, there is a continuous energy loss is associated with this technique due to its boil-off. Even though the current technique using a special container with the volume of 15 m^3 is adopted, 0.7 % amount of hydrogen is lost per day [4].

1.2.3 Storage materials

To realize the high condensed and safe state of hydrogen, a lot of researchers have focused on the solid state hydrogen storage materials. As according to the different storage states, the hydrogen storage materials are classified to physisorption type, in which hydrogen is adsorbed on a surface as a molecule state, and chemisorption type, in which hydrogen is absorbed in a bulk as an atomic state. In the case of physisorption,

the condensed hydrogen state is realized by using the interaction between H_2 and material surface due to the effect of Van der Waals' forces. Thus, the materials with high surface area and high pore volume are basically useful. The phenomenon makes the occupied volume to be extremely lower than that of gaseous state. For example, the metal-organic frameworks (MOFs) are recognized as a novel trend on hydrogen storage. In 2003, Rosi *et al.* reported that one of MOFs can physically absorb hydrogen up to 4.5 wt.% at 77 K under 2 MPa H_2 [5]. However, the interaction of physical absorption is extremely weak, so an ultralow temperature is necessary to obtain large enough amount of hydrogen. In fact, it was reported that the amount of absorbed hydrogen at room temperature was only 1.0 wt.%.

The hydrogen storage materials by chemisorption can absorb large amount of hydrogen even at room temperature, where they are generally called as hydrides. So far, various kinds of materials have been proposed and studied as hydrogen storage materials for especially on board application. The capacity and properties of hydrogen absorption and desorption strongly depend on the materials as introduced from next section.

1.3   Basic principles

In order to control hydrogen storage materials, thermodynamics and kinetics are important parameters. The basic principles of them are described below.

1.3.1 Thermodynamics

The thermodynamics of metal-hydrogen, *M*-H, systems are understood by the phase diagram shown in Fig. 1-1(a) [6]. This figure is called PCIs or PCT chart because

they are originated by the three factors, which are hydrogen pressure, concentration of hydrogen in the system, and the temperature of the system. The hydrogen absorption and desorption to metals proceeds as gas-solid reaction. From experimental point of view, the phase diagram is accomplished by measuring the variation of hydrogen pressure and concentration in the metal under isothermal conditions. About each isothermal line under the critical point denoted as Tc in Fig. 1-1(a), the state of solid phase is changed depending on the concentration of hydrogen. The hydrogen solution state denoted as α phase is observed in the region of low hydrogen concentration. The crystal structure is not so different from that of pure metal, because hydrogen atoms is dissolved into the interstitial sites of crystal structure. The schematic view of hydrogen self-trapping is shown Fig. 1-2 [7]. When a hydrogen atom is located into the interstitial site formed by metal atoms, the metal lattice is expanded by the repulsive forces between metal and hydrogen atoms as shown in Fig. 1-2(a). The potential energy change by this phenomenon is shown in Fig. 1-2(b). The total potential energy, E, is approximated by addition of E_L and E_0. Here, E_L and E_0 are the potential energy for the lattice deformation of metals and the potential energy of the ground state for hydrogen, respectively. E_L is increased with the displacement of the lattice atoms. Inversely, E_0 should be decreased by decline of the repulsive force between metals and hydrogen. Consequently, the lattice atoms were automatically displaced to the point μ^*. In other words, the stable potential site for hydrogen is formed by hydrogen itself. This phenomenon is called as "Self-trapped state". As the concentration of hydrogen atoms in the solid state is increased, a stable hydride phase (β phase) is locally generated as a new phase because of the large deformation of the metal lattice and the repulsion of other hydrogen atoms. Thus, two kinds of solid phases coexist, where this state is

denoted as α+β in Fig. 1-1(a). In this region, with introducing hydrogen, the ratio of α and β phases is changed. As a result, the hydrogen pressure is constant despite the increase in hydrogen concentration. This phenomenon is understood by the Gibbs' phase rule described as follows,

$$F = C - P + 2, \qquad\qquad (1\text{-}1)$$

where F is the degree of freedom, C is the number of components, and P is the number of phases in the reaction system. In the α+β coexistence state, the C and P are 2 (metal and hydrogen) and 3 (α, β, and gaseous H_2), respectively, resulting is $F = 1$, namely, the hydrogen pressure is fixed at a constant value with concentration variation under isothermal condition. This pressure is generally called as "plateau pressure". The plateau range has a very important role for the application of hydrogen storage. The pressure at the temperature is the operating hydrogen pressure, and the length of plateau region corresponds to the available hydrogen amount as a hydrogen storage. After the plateau region, the pressure is increased again. This region is denoted as β in Fig. 1-1(a). For hydrogen storages, the equilibrium state is important to control hydrogen absorption and desorption properties. The equilibrium pressure is directly related to the enthalpy change of the M-H system. The flat plateau pressure is a principal factor for practical application because the hydrogen absorption and desorption should be controlled by supplying and removing the hydrogen pressure.

The thermodynamics of above M-H reactions is described on the basis of free energy of chemical reaction as follows. Under the equilibrium condition, the both chemical potentials before and after the reaction should be equal because the reversible reactions proceeds in the equilibrium state.

For the solid solution state (α phase), the equilibrium state is described as the

6

following equation,

$$M + \frac{x}{2}H_2 \Leftrightarrow MH_x,$$ (1-2)

where x is the number of hydrogen atoms dissolved in solid state. The indispensable condition for this equilibrium state is expressed by the chemical potentials of the hydrogen in both sides of reaction as follows,

$$\frac{1}{2}\mu^g = \mu^\alpha,$$ (1-3)

where μ^g and μ^α are the chemical potential of gaseous hydrogen, H_2, per molecule and the hydrogen atom, H, dissolved in metal per atom, respectively. The μ^g is regarded as an ideal gas under low pressure and described as

$$\mu^g = kT \ln \frac{p}{p_0(T)} - E_d,$$ (1-4)

$$P_0(T) = \frac{32(\pi^7 k^7 M^3 T^7)^{1/2} I_r}{h^5},$$ (1-5)

where k, T, p, E_d, h, M, and I_r are the Boltzmann constant, temperature, gaseous hydrogen pressure, dissociation energy of hydrogen molecule, Planck's constant, mass of hydrogen atom, and inertia moment of hydrogen molecule, respectively. In the case of considering the chemical potential only from contribution of the pressure, the standard pressure, p_0, is a constant value, 1 atm (0.1013 MPa). The μ^α is given by the Gibbs free energy, G, and the relation between each other is represented as

$$\mu^\alpha = \frac{\partial G^\alpha}{\partial x},$$ (1-6)

where G^α is the Gibbs free energy of solid solution state, and x is the number of hydrogen atoms in solid solution state shown in equation (1-2). And the Gibbs free

7

energy is defined by the enthalpy, H, and entropy, S, as follows,

$$G = H - TS. \tag{1-7}$$

So, G^{α} can be described as same as the equation (1-7) by using H^{α}, and S^{α}, where they are the enthalpy and entropy of solid solution, respectively. H^{α} is constituted by the partial enthalpy, h^{α}, which is attributed between the dissolved hydrogen atom and metal atoms. The S^{α} is constituted by the configuration and the non-configuration parts. The configurational entropy, S^{c}, is attributed by the position of dissolved hydrogen atoms on the interstitial sites. And the non-configuration entropy, S^{nc}, contains other factors such as the vibrational and electronic contribution, which is originated by the partial interaction between the dissolved hydrogen and metal atoms. Here, the number of the interstitial sites and the partial enthalpy per a metal atom are shown as N and h^{α}, respectively, and then H^{α} and S^{α} are described as follows,

$$H^{\alpha} = xh^{\alpha}, \tag{1-8}$$

$$S^{\alpha} = S^{c} + S^{nc}, \tag{1-9}$$

$$S^{c} = k\ln({}_{N}C_{x})$$

$$= k\ln\left(\frac{N!}{x!(N-x)!}\right), \tag{1-10}$$

$$S^{nc} = xs^{nc}. \tag{1-11}$$

G^{α} is divided into the two parts, which are the configurational and non-configurational terms, and then G^{α} is able to described as

$$G^{\alpha} = G^{\alpha nc} + G^{\alpha c}$$

$$= G^{\alpha nc} - TS^{c}, \tag{1-12}$$

because H is not related to the configurational factors. From equation (1-6), (1-7), and (1-12), the μ^{g} is described as follows,

$$\mu^{\alpha} = \frac{\partial G^{\alpha}}{\partial x} = \frac{\partial G^{\alpha nc}}{\partial x} - kT \frac{\partial S^{c}}{\partial x}.$$

(1-13)

Here, the last term of equation (1-13) is changed by the Stirling's apploximation as follows,

$$\ln(n!) \approx n\ln n - n,$$

(1-14)

and described as

$$kT \frac{\partial S^{c}}{\partial x} = kT \frac{\partial}{\partial x}\left\{ \ln\left(\frac{N!}{x!(N-x)!}\right)\right\} \approx kT \ln\frac{N-x}{x}.$$

(1-15)

Therefore, the equation (1-13) is written as

$$\mu^{\alpha} \approx \mu^{\alpha nc} - kT \ln\frac{N-x}{x} = h^{\alpha} - Ts^{nc} + kT \ln\frac{x}{N-x}.$$

(1-16)

As the result, the condition to be the equilibrium state of hydrogen solution state is described by the equations (1-3), (1-4), and (1-16) as follows,

$$kT \ln\left(\frac{p}{p_0(T)}\right)^{1/2} - \frac{1}{2}E_d = h^{\alpha} - Ts^{nc} + kT \ln\frac{x}{N-x}.$$

(1-17)

When the dissolved hydrogen is relatively lower level, i.e. in the case of $x \ll N$, the last term of the equation (1-17) can be approximated as follows,

$$kT \ln\frac{x}{N-x} \approx kT\left(\ln x - \ln N\right).$$

(1-18)

Finally, the relation between the x and p is obtained as follows,

$$x = K_s\left(\frac{p}{p_0}\right)^{1/2},$$

(1-19)

$$K_s = N \exp\left(\frac{Ts^{nc} - h^{\alpha} - \frac{1}{2}E_d}{kT}\right).$$

(1-20)

9

The relation expressed by equation (1-19) is called as "Sieverts' law" and is able to be observed in various M-H systems. The value of H^{α} depends on the metals. The enthalpy changes corresponding to the formation of solid solution, ΔH_s^0, are shown in Table 1-1 [7]. ΔH_s^0 has not only positive value but also negative value depending on the metals. For example, for Mg, the ΔH_s^0 is negative value, suggesting that the solid solution between Mg and hydrogen is difficult to be formed.

For the coexistence region of α and β phases shown in Fig. 1-1, the equilibrium reaction to form hydride is described as same as the equation (1-2). The variation of Gibbs free energy is generally expressed by the following equation,

$$dG = dH - TdS - SdT .$$
(1-21)

Here, H is defined with the internal energy, U, and describe as follows,

$$H = U + pV ,$$
(1-22)

and

$$dH = dU + pdV + Vdp ,$$
(1-23)

where V is the volume. When the total energy is not changed in system, dU can be expressed as follows,

$$dU = TdS - pdV .$$
(1-24)

And, the equation (1-21) is expressed by substitution of the equations (1-23) and (1-24),

$$dG = Vdp - SdT .$$
(1-25)

In the case of the reaction between α and β phases shown in Fig. 1-1 performed in isothermal condition, the Gibbs free energy is expressed as a function of the pressure,

and it can be described as follows when the pressure is changed from p_i to p_f,

$$G(p_f) = G(p_i) + \int_{pi}^{pf} V dp$$

$$= G(p_i) + nRT \int_{pi}^{pf} \frac{dp}{p} \quad \left(\because pV = nRT \right). \tag{1-26}$$

When p_i is the standard pressure (p_0), the equation (1-26) is described as follows,

$$G(p) = G_0 + nRT \ln\left(\frac{p}{p_0} \right), \tag{1-27}$$

where G_0 is the Gibbs energy in the standard state. Therefore, the equilibrium condition under the pressure, p_{eq}, is expressed as following relation by substitution of the equation (1-7),

$$\ln\left(\frac{p_{eq}}{P_0} \right) = \frac{\Delta H}{RT} - \frac{\Delta S}{R}, \tag{1-28}$$

where ΔH and ΔS are the variations of the enthalpy and entropy in the reaction, respectively. This equation is called "van't Hoff equation", and the figure shown by the pressure versus the inverse of temperature is called "van't Hoff plot" shown in Fig. 1-1(b). The ΔH and ΔS of reaction are represented by the slope and intercept of plots, respectively. The values are shown in Table 1-2.

Basically, the equilibrium pressures for hydrogen absorption and desorption reactions should be the same value in ideal model because enthalpy and entropy changes are not changed. However, there is difference in equilibrium pressure for the practical situation. During the hydrogen absorption process, a plastic deformation occurs by forming the hydride phase, therefore, the thermodynamic equilibrium

11

conditions is slightly shifted due to a generation of the lattice defects and deformation. As a result, the equilibrium pressure of hydrogen absorption process is higher than that of desorption process. Thus, the hydrogen desorption process is generally analyzed to estimate the enthalpy and entropy change for the reaction because the contribution of above deformation is lower than that of hydrogen absorption.
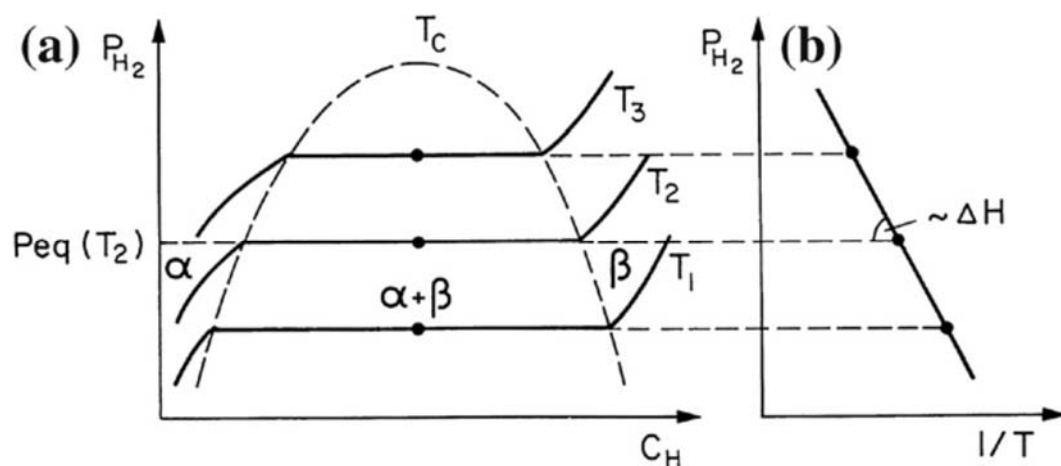
Figures 1-1 (a) PCIs chart for hydrogen absorption and desorption of a metal, and (b) van't Hoff plot for the obtained pressure and temperature [6].
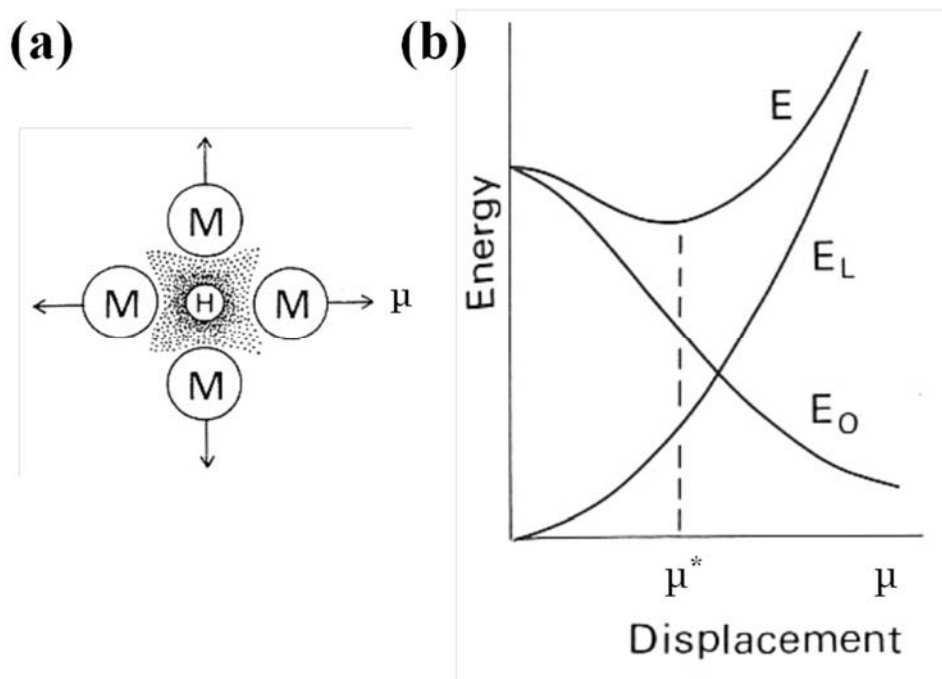
Figure 1-2 Schematic diagrams for the physics of hydrogen self-trapping effect. (a) Scheme for the hydrogen self-trapping phenomenon. (b) Energy diagram of each potential energy against the displacement of lattice metals. [7]

Metal	ΔH_s^0 [eV per atom]	$\Delta S_s^0/k$	T [°C]
Li	-0.54	-7	200–700
Mg	$+0.22$	-4	500
Al	$+0.70$	-6	500
Sc	-0.94	-7	–
Y	-0.85	-6	–
La (fcc)	-0.83	-8	–
Ce (fcc)	-0.77	-7	–
Ti (hcp)	-0.55	-7	500–800
Ti (bcc)	-0.62	-6	900–1100
Zr (hcp)	-0.66	-6	500–800
Zr (bcc)	-0.67	-6	860–950
Hf (hcp)	-0.38	-5	300–800
V	-0.28	-8	150–500
Nb	-0.35	-8	>0
Ta	-0.39	-8	>0
Cr	$+0.60$	-5	730–1130
Mo	$+0.54$	-5	900–1500
W	$+1.1$	-5	900–1750
Fe (bcc)	$+0.25$	-6	<900
Ru	$+0.56$	-5	1000–1500
Co (fcc)	$+0.33$	-6	1000–1492
Rh	$+0.28$	-6	800–1600
Ir	$+0.76$	-5	1400–1600
Ni	$+0.17$	-6	350–1400
Pd	-0.10	-7	-78–75
Pt	$+0.48$	-7	–
Cu	$+0.44$	-6	<1080
Ag	$+0.71$	-5	550–961
Au	$+0.37$	-9	700–900
U (α)	$+0.10$	-6	<668

Table 1-1 The standard enthalpy and entropy changes to form a hydrogen solid solution in the low concentration of dissolved hydrogen, and the temperature condition of experiments performed. [7]

14

	ΔH (kJ/mol H_2)	$\Delta S^0/R$ (mol H_2)$^{-1}$	Temperature range (°C)
Li–LiH	−158	−16.2	600–900
Na–NaH	−114	−19.6	500–600
K–KH	−118	−20.2	288–415
Rb–RbH	−108	−20.4	246–350
Cs–CsH	−114	−20.4	245–378
Mg–MgH$_2$	− 74	−16.0	440–560
Ca–CaH$_2$	−182	−16.8	600–800
Sr–SrH$_2$	−198	−18.8	<1000
Ba–BaH$_2$	−174	−17.2	470–550
Sc–ScH$_2$	−200	−17.4	>600
Y–YH$_2$	−226	−17.4	600–950
YH$_2$–YH$_3$	−178	−16.6	250–350
La–LaH$_2$	−208	−18.2	600–800
LaH$_2$–LaH$_3$	−168	—	—
Ce–CeH$_2$	−206	−17.8	600–800
CeH$_2$–CeH$_3$	−238	—	—
Pr–PrH$_2$	−208	−17.6	600–800
Nd–NdH$_2$	−212	−17.6	650–840
Sm–SmH$_2$	−222	−19.6	—
Gd–GdH$_2$	−196	−15.8	600–800
Er–ErH$_2$	−226	−18.8	—
Ti(hcp)–TiH$_2$	−130	−12	<300
Zr(hcp)–ZrH$_2$	−188	−18	400–550
Hf(hcp)–HfH$_2$	−130	−12	600–900
V–VH$_{0.5}$	− 72	−13	0–100
V–VH$_2$	− 40	−18	50–120
Nb–NbH$_{0.65}$	− 92	−16	0–80
Nb–NbH$_2$	− 40	−16	25
Ta–TaH$_{0.5}$	− 78	−12	<50
Mn(a)–MnH	− 22	−14*	450–730
Ni–NiH	− 58	−14*	20
Pd–PdH$_{0.5}$	− 40	−10	−78–175
Mg$_2$Ni–Mg$_2$NiH$_4$	− 64	−14.4	—
TiFe–TiFeH	− 28	−12.4	—
CaNi$_5$–CaNi$_5$H$_4$	− 34	−12.2	—
LaNi$_5$–LaNi$_5$H$_4$	− 32	−13	—

Table 1-2 The heat of formation and standard entropy of metal hydrides, and the temperature conditions of experiments performed [8].

15

1.3.2 Kinetics

The reaction kinetics is controlled by only rate-determining step. The theory of reaction between hydrogen and metals is understood by the potential energy scheme shown in Fig. 1-3 [9]. The x axis shows the distance between hydrogen and metal, and the y axis shows the total potential energy of each state. This figure is called "one-dimensional Lenenard-Jones potential" and utilized to understand the mechanism of typical gas-solid reaction. In this model, some kinetic energy barriers exist for the reaction progress. In general, the absorption reaction between gaseous hydrogen and metals consist of the following four steps,

    i.   Adsorption step: a gas molecule collides to the solid surface, and the molecule is physisorbed on the surface.

    ii.   Chemisorption step: the adsorbed molecule dissociates to the atoms on the solid surface.

    iii.   Diffusion step: the atoms is moved and diffused into a inter layer of solid bulk.

    iv.   Hydride formation step: some chemical bonds are formed, and the crystal structure is transformed.

The rate-determining step of the reaction is controlled by one of these steps. Thus, in order to improve the kinetics of the reaction, it is required to understand which step is the rate-determining step and how to decrease the saddle point of the potential energy.

The adsorption and chemisorption steps are described as the sum of interaction energy between the hydrogen and metal as shown in the gas and interface regions of Fig. 1-3. For the detail of this region, the hydrogen state is separated to a molecule and

16

atoms, and the qualitative interaction energy between each hydrogen and metal are shown in Fig. 1-4 [8]. The figures indicate the interaction energy, U, between hydrogen molecule or atom and metal versus the distance between hydrogen and metals, Z. Fig. 1-4(a) shows the relation when hydrogen molecule is approaching to the metal surface. When the Z is decreased, the attractive force by the van der Waals' force acts to stabilize the potential energy, and then U is decreasing. However, when Z is furthermore decreased, the electron repulsion between the hydrogen molecule and metal becomes as a dominant factor, and then U is increasing. The minimum value is appeared, and this stabilization is called as "physisorption effect" denoted as E_p. The effect is temporary in the whole M-H reaction, therefore the extremely low temperature condition is required to keep the state for a long time because the adsorption energy is generally small (3~15 kJ/mol H_2 [8]). Fig. 1-4(b) shows the relation between hydrogen atoms and metal. When the distance between hydrogen atom and metal is far enough, U takes a large value because a large amount of energy is required for dissociation of hydrogen molecule. As Z is decreasing, a covalent orbital appears between hydrogen atom and metal, which leads to the "chemisorption effect" denoted as E_{ch}. This effect is much larger than that of physisorpion, namely, E_{ch} appears as the stable sate on the reaction. However, for the metals which have only poor spread of valance electrons, the covalent orbital between hydrogen and metals is hard to be formed, and then hydrogen dissociation is not occurred. Fig. 1-4(c) is obtained by the addition of (a) to (b). By the position of intersection for two potential curves, P, the adsorption process is classified to following schemes shown in Fig. 1-4(d) and (e). When P takes a value under zero, the energy scheme is shown as Fig. 1-4(d). The hydrogen atom achieves to be the stable chemisorpion state through the adsorption step without activation because

U is under zero value during the process. On the other hand, If P is above zero value, the activation energy, E^*_{ad}, is required to form the chemisorption state as shown in Fig. 1-4(e). The diffusion step of hydrogen atoms is expressed by thermal process. The hydrogen atoms trapped in the potential valley, e.g. the interstitial site, are able to jump from the potential valley to the neighbor site by the lattice vibration of metals due to thermal energy. Regarding the hydride formation step, hydrogen and metal atoms are necessary to move the comfortable position, namely, the thermal energy is required to rearrange the atoms as well as the diffusion step. Therefore, these two steps are thermal active processes. Regarding the energy distribution at some temperature, *T*, the probability to pass the potential barrier is described as following equation, where *k* is the Boltzmann constant. And, the kinetic coefficient of reaction, *K*, is able to be described as

$$K = K_0 \exp\left(\frac{-E}{RT}\right),$$
(1-29)

where K_0 is the frequency factor, and *E* is the activation energy. The equation is able to be transformed as follows,

$$\ln K = \frac{-E}{RT} + \ln K_0.$$
(1-30)

This equation is called "Arrhenius equation", and it is important to estimate the activation energy by experimental results. According to the plot of reaction rate versus the inverse of temperature, the activation energy and the frequency factor can be estimated from the gradient and the intercept, respectively.
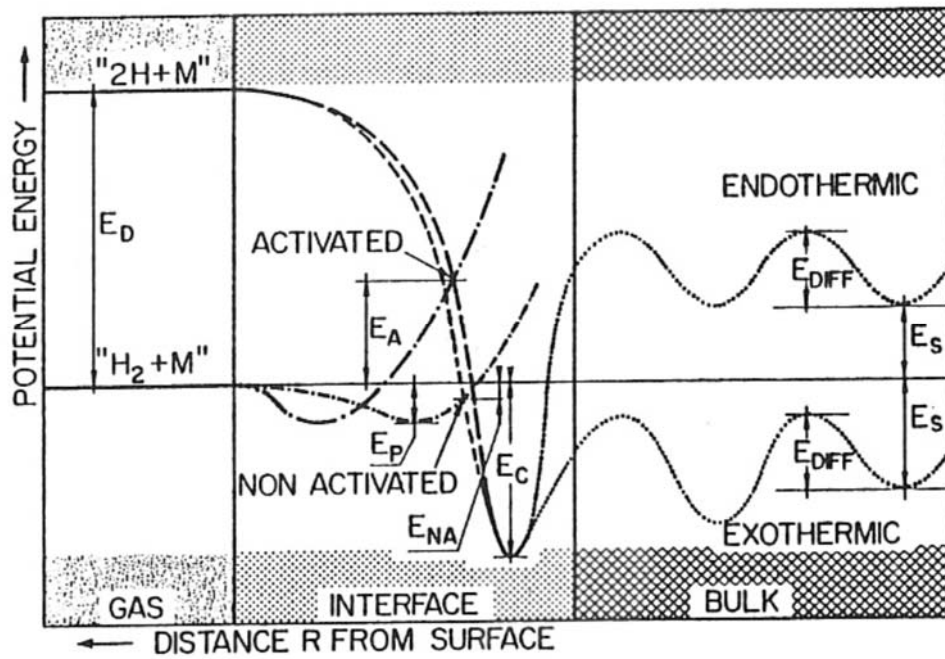
Figure 1-3 The total potential energy curves of hydrogen and metal versus the distance
between hydrogen and metal surface [9].
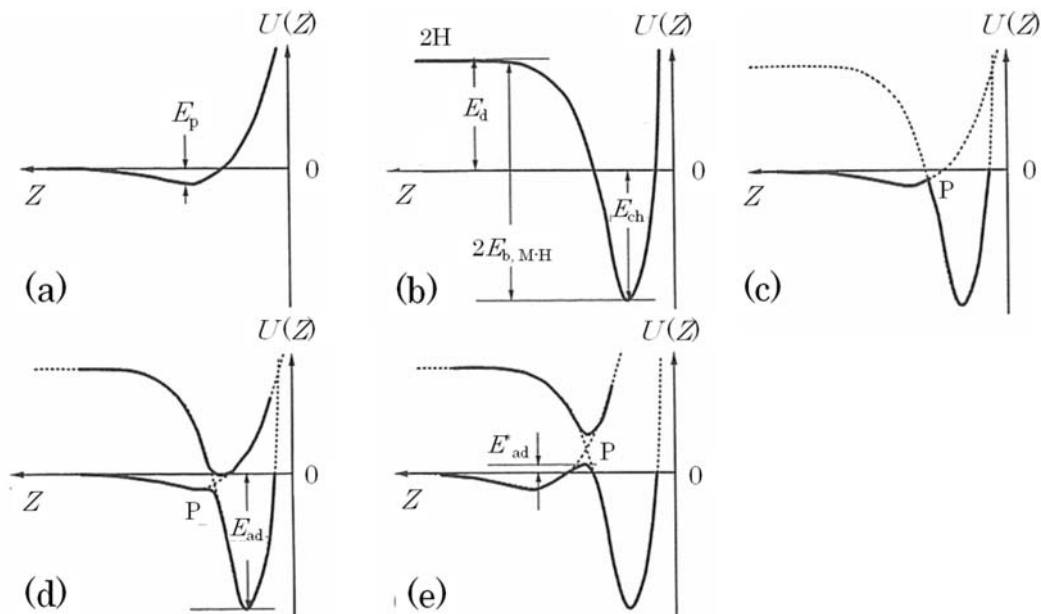
Figure 1-4 The interaction energy between hydrogen and metals versus the distance
between hydrogen and metal surface [8]

1.4   Hydrogen storage materials

The hydride state can be distinguished by the variety of chemical bonding between hydrogen and the materials, which is attributed to the following factors.

A)   The electronegativity of hydrogen is neutral position in all the elements. The electronegativity is the degree of easiness to attract an electron toward the nucleus, and χ is widely used as the symbol. If the relationship of the electronegativity between A and B is described as $\chi_A < \chi_B$, the electrons is transferred from A to B, and the electron state would be changed to the nearly state described as A^+B^-. If the relation of the electronegativities between A and B is $\chi_A \approx \chi_B$, the bonding formed without charge transfer.

B)   Hydrogen should be the smallest size of all elements because it possesses only the smallest electron orbital. The size of electron orbital is changed with its charge state. The protide, H^-, has the largest ionic radius of 2.1 Å in the three states of hydrogen, and the value is comparable to heavy halogens (1.95 Å for Br^- and 2.16 Å for I^-). The size of a protium, H^0, is measured in Bohr radius that is 0.529 Å. H^+ is constituted by just only one proton, and the size is noteworthy negative value as −0.18~0.38 Å [7].

C)   Hydrogen has the smallest mass of all elements. This mass effect is especially appeared for the diffusion step after dissociating the molecules. Regarding hydrogenation in alloys, there are no-charge transfer as described below, then the mass is dominated a majority factor for the diffusion reaction.

The bonding types of hydrides are classified into three categories: ionic, covalent, and

metallic states. The bonding states of hydrides are mainly affected by the valance electrons of metals, namely the interaction between hydrogen and metals are roughly distinguished by the area in the periodic table shown in the table 1-3 [8].

1A	2A	3A	4A	5A	6A	7A	8A			1B	2B	3B	4B	5B	6B	7B
H 2.1													non-metal			
Li 1.0	Be 1.5					metal						B 2.0	C 2.5	N 3.0	O 3.5	F 4.0
Na 0.9	Mg 1.2					transition metal						Al 1.5	Si 1.8	P 2.1	S 2.5	Cl 3.0
K 0.8	Ca 1.0	Sc 1.3	Ti 1.5	V 1.6	Cr 1.6	Mn 1.5	Fe 1.8	Co 1.8	Ni 1.8	Cu 1.9	Zn 1.6	Ga 1.6	Ge 1.8	As 2.0	Se 2.4	Br 2.8
Rb 0.8	Sr 1.0	Y 1.2	Zr 1.4	Nb 1.6	Mo 1.8	Tc 1.9	Ru 2.2	Rh 2.2	Pd 2.2	Ag 1.9	Cd 1.7	In 1.7	Sn 1.8	Sb 1.9	Te 2.1	I 2.5
Cs 0.7	Ba 0.9	La-Lu 1.1−1.2	Hf 1.3	Ta 1.5	W 1.7	Re 1.9	Os 2.2	Ir 2.2	Pt 2.2	Au 2.4	Hg 1.9	Tl 1.8	Pb 1.8	Bi 1.9	Po 2.0	At 2.2
		Ac 1.1	Th 1.3	Pa 1.5	U 1.7											

Table 1-3 The periodic table with the hydride categories [8]

1.4.1 Ionic hydrides

Regarding the alkali (1A group in the Table 1-3) and alkaline-earth (2A group in the Table 1-3 excluded Be and Mg) metals, the electronegativity of metal is much lower than that of hydrogen, which causes the valence electrons of metal are attracted toward hydrogen to stabilize each electron orbital. In the case of beryllium and magnesium, the hydride bond is regarded as a covalent state rather than the ionic one, because the differences of the electronegativity between hydrogen and metals are lower than those of other elements in 1A and 2A. The main driving force to make the ionic crystal structure is electrostatic force, namely, hydrogen becomes a protide-like state by receiving an electron, and the metal atom becomes a cation-like state by loss of

electrons.

1.4.2 Covalent hydrides

When the electronegativity of hydrogen is almost same or lower value than those of other elements, the covalent bonding is formed with the elements shown in region from 3B to 7B in the table 1-3. The bonding has a polar property corresponding to the difference of electronegativity between the two elements, for example of water, the each elemental state is described as $H^{\delta+}$ and $O^{\delta-}$, respectively. On the other hand, in the case that the elements which have nearly electronegativity of hydrogen, the polymeric molecule is formed by bridging bond such as B_2H_6 and $(AlH_3)_3$. The covalent hydrides have some attractive properties, which are high theoretical hydrogen capacity and the liquefaction state under moderate conditions such as methane (CH_4) and ammonia (NH_3). Therefore, the covalent hydrides have been researched for practical use as hydrogen storage. In the sections 1.4.5 and 1.4.6, the properties of organic hydrides and ammonia are described.

1.4.3 Complex hydrides

Complex hydrides, which are described as $M(XH_m)_n$, are composed by metal cations and complex anions such as $(NH_2)^-$, $(BH_4)^-$, and $(AlH_4)^-$. The metal cations are typically alkali and alkaline-earth elements. For the complex anions, the covalent bondings are formed between hydrogen and the elements shown in the region from 3B to 5B in the table 1-3. The theoretical hydrogen capacity is relatively high (18.5 mass% for $LiBH_4$) from that of typical light metal hydride such as MgH_2 (7.6 mass%). The interactions between the metal cation and the complex anion are strongly depended on

22

the M and X elements. As a result, some complex hydrides desorb not only H_2 but also some other gaseous during the thermal decomposition. Actually, when amides described as $M(NH_2)_n$ are decomposed, NH_3 is desorbed with some reaction steps [10]. Thus, in order to utilize the complex hydrides for hydrogen storages, the reaction process has been investigated so far. For example, $LiBH_4$, which is regarded as attractive material among complex hydrides, is thermally decomposed by the following processes [11].

$$LiBH_4 \rightarrow LiBH_{4-x} + \left(\frac{x}{2}\right)H_2 \qquad \text{(0.3 mass\% of hydrogen, till 110 °C)}$$

$$LiBH_{4-x} \rightarrow LiBH_2 + \left(\frac{1-x}{2}\right)H_2 \qquad \text{(8.7 mass\% of hydrogen, till 480 °C)}$$

$$LiBH_2 \rightarrow LiH + B + \left(\frac{1}{2}\right)H_2 \qquad \text{(4.5 mass\% of hydrogen, over 600 °C)}$$
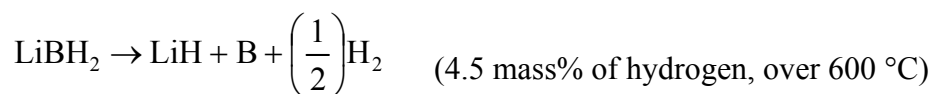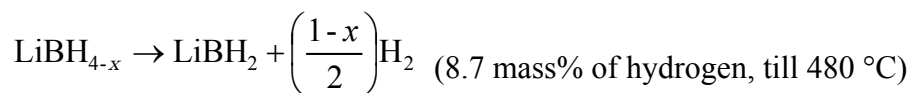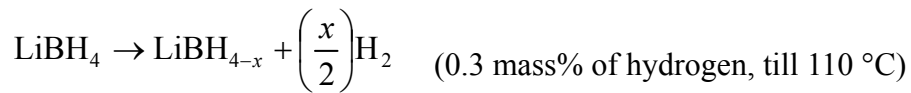
1.4.4 Metallic hydrides

For the transition metals (3A~8A in the Table 1-3, and Pd), the metallic hydrides are formed with various kinds of bonding. Regarding the elements shown 3A~5A in the Table 1-3, the hydrides are interstitial type as mentioned 1.3.1. The enthalpy change for hydrogen absorption process is negative value, namely, the hydride phase is stable. In the case of the elements shown in 6A~8A groups excluded Pd in the Table 1-3, the hydrides are formed with hydrogen atom as proton state by the weak interaction between both elements, and then the hydride phase is unstable. Namely, although hydrogen is able to diffuse during the metallic phase, the hydride phase is not formed. The metallic hydrides are formed by the reaction between hydrogen and alloys.

For practical use of hydrogen storage materials especially for on-board application, a high hydrogen capacity and low equilibrium pressure which is about from 0.1 MPa to 1.0 MPa at room temperature are required. For the alloys, the control of thermodynamic and kinetic properties is relatively easier than the ionic and covalent hydrides. Above properties can be modified by substituting the elements included in the alloys by the other elements, suggesting that the equilibrium hydrogen pressure can be controlled to be suitable one. The hydrogen storage alloys are basically composed by A metals, which possesses a high affinity with hydrogen, and B metals, which possesses a low affinity metal. The compositions of alloys are categorized to following four groups: AB type, AB_2 type, AB_5 type, and A_2B type. Here, for practical use of hydrogen storage alloys, high pressure MH tank as shown in Fig1-5, which was combined the high pressure cylinder with alloys, was proposed [12]. This system shows excellent thermodynamic, kinetic properties, and the capacity is larger than that of only compressed hydrogen at the same pressure.
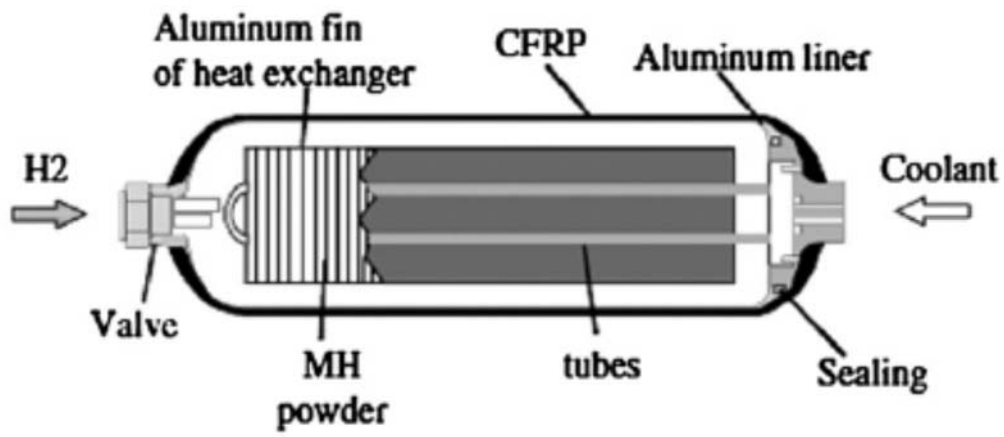
Figure 1-5 Schematic figure of high-pressure MH sylinder [12].

1.4.5 Organic hydrides

The organic hydride systems are considered for the massive storage and transportation as liquid hydrogen carrier, which is attractive from practical point of view because the infrastructure for fossil fuels is possibly utilized. The reactions of various organic hydride systems and gravimetric/volumetric hydrogen density are shown in the Table 1-4 [13]. The hydrogen density is comparable with that of typical light metal hydrides such as 7.6 wt% for MgH_2. In addition, organic hydrides are liquid state at room temperature under atmospheric pressure conditions, indicating that they are regarded as a useful energy medium due to their behavior close to the oil. However, thermal energy is necessary for hydrogenation process even by the exothermic reaction. Furthermore, the separation between generated H_2 and vapor of organic material is required to obtain a high purity H_2.

Table 1-4 Chemical reactions of naphthalene ($C_{10}H_8$), decahydronaphthalene ($C_{10}H_{18}$), and benzene (C_6H_6) for hydrogen absorption and desorption, and hydrogen capacities [13].

Reaction	Hydrogen density	
	wt%	kg/m^3
$C_{10}H_8+5H_2 \leftrightarrow C_{10}H_{20}$	7.3	65
$C_6H_6+3H_2 \leftrightarrow C_6H_{12}$	7.1	55
$C_7H_8+3H_2 \leftrightarrow C_7H_{14}$	6.2	48

1.4.6 Ammonia

In recent years, ammonia has also been projected as a hydrogen carrier for storage and transportation because of the following attractive properties [12]:

A.   gravimetric hydrogen capacity is high, 17.8 mass%

B.   high volumetric density (107.3 kg H_2/m^3 at room temperature) of hydrogen is realized by liquefaction at 20 °C under 0.86 MPa, and it is higher than that of liquid hydrogen at -253 °C under 0.1 MPa (around 71 kg/m^3)

C.   infrastructures for transportation and storage are established

However, high temperature over 400 °C is required for decomposition of ammonia to obtain hydrogen even if Ru-based catalysts are used [14, 15]. A new reaction concept between ammonia and hydrides shown as following expression, has been proposed, and the hydrogen is reversibly absorbed and desorbed at a mild conditions compared with NH_3 itself,

$$MH + NH_3 \leftrightarrow MNH_2 + H_2 \ (M=\text{Li, Na, K}) \ [16, 17]. \qquad (1\text{-}31)$$

In the case of the Li system, 8.1 mass% hydrogen can be derived at room temperature, and a heat less than 300 °C is only required for the inverse reaction.

1.5　Magnesium hydride

Mg has been researched as a typical hydrogen storage material in several decades. Mg can reversibly absorb and desorb large amount of hydrogen (7.6 wt.%) by following reaction,

$$Mg + H_2 \leftrightarrow MgH_2, \qquad (1\text{-}32)$$

Also, it is a cheap material due to its abundance in nature. However, it has disadvantageous properties. First one is the high enthalpy change, 74 kJ/mol which is still high for practical use although it is relatively small value among light metal hydrides as shown in Table 1-2. Thermodynamically, the hydrogen desorption requires 300 °C to obtain 0.1 MPa of H_2. Second one is poor kinetics. Because, the Mg surface is inactive for the dissociation of hydrogen molecule, indicating that the activation barrier exists in the dissociation step. Thus, many researchers have investigated to improve above properties.

For thermodynamics improvement, the synthesis of alloys with other elements is effective method. In the 1960s, Mg-transition metals alloys were discovered such as Mg-copper [18] and Mg-nickel [19] alloys. The enthalpy changes were estimated as 72.9 kJ/mol and 64.5 kJ/mol for Mg_2Cu and Mg_2Ni alloy, respectively. These values are lower than 74.9 kJ/mol for pure Mg [20]. Although the capacity of hydrogen was lower than that of pure Mg, the thermodynamics and kinetics were improved. Furthermore, the composite system between MgH_2 and borohydrides was proposed by Vajo *et al*. where the hydrogen abosorption and desorption proceeded as following equation,

$$2LiH + MgB_2 + 4H_2 \leftrightarrow 2LiBH_4 + MgH_2. \qquad (1\text{-}33)$$
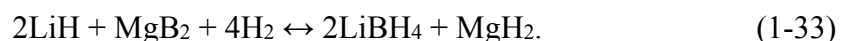
The enthalpy change corresponding to the reaction i.e. 40.5 kJ/mol, is lower than that of pure Mg. In addition, the capacity of hydrogen storage is able to keeps high level i.e. 8.5

28

wt.% [21].

The improvement of kinetic properties for the reactions of Mg has been studied by many researchers as well. Here, the rate-determining step for hydrogen absorption of Mg is regarded as follows. The dissociation of hydrogen molecules to atomic state is an important step because this is the initial step of the hydrogen absorption reaction. The valence electrons in Mg are attributed to $3s$ orbital, which are localized around nucleus. As a result, the dissociation of hydrogen molecules is unfavorable. As another problem, it was reported that the growth of Mg hydride layer is prevented by its own [22]. The authors claimed that the diffusion of the Mg hydride in Mg is affected by the hydrogen pressure. Thus, for the hydrogenation reaction of Mg, it is expected that either reaction step is recognized as the rate-determining step.

For improving the hydrogen sorption kinetics, mechanical milling for MgH_2 or Mg is highly effective [23, 24]. Zaluska *et al*. demonstrated that the enhancement of hydrogen absorption amount for Mg was effected by decreasing the crystal grain size, and they concluded that the ball milling introduced a lot of defects and grain boundaries. These structural properties affected the nucleation of MgH_2 and the improvement of H diffusion [23]. Huot *et al*. reported that a part of MgH_2 phase was changed to a metastable orthorhombic phase (γ phase) from a stable tetragonal phase (β phase) by ball milling for only 2 hours, and the crystalline size of β phase was decreased [24]. Thus, the ball-milling effects for hydrogenation reaction of pure Mg are summarized as the nucleation of MgH_2 by making the metastable phase and the diffusion of H atoms by addition of some defects and grain boundaries.

For further improvements of the kinetics, many catalysts have been added to Mg, and their properties were investigated. 5 mol% $3d$-transition metals (Ti, V, Mn, Fe, and

Ni) were added as the catalyst to Mg by Liang *et al.*, and Ti has been found as the most active catalyst for hydrogen absorption reaction of Mg, while V is the most effective catalyst among them for the hydrogen desorption reaction [25]. For the other $3d$-transition metals (Cu, Fe, Co, and Ni), Hanada *et al.* investigated the catalysis for the hydrogen desorption process. As a result, Ni has better catalytic effect for the hydrogen desorption reaction of MgH_2 among these four transition elements [26].

In general, the tradition metals are effective for dissociation of hydrogen molecules because the tradition metals have *d*-orbital electrons, which have the wide extent of wave function and easily interact with the bonding of H_2. It is noteworthy that the transition metal oxides were also recognized as excellent catalysts for the Mg-H system. In study by Oelerich et al., some metal oxides (Sc_2O_3, TiO_2, V_2O_5, Cr_2O_3, Mn_2O_3, Fe_3O_4, CuO, Al_2O_3, and SiO_2) were added to Mg as the catalysts. They compared the properties of hydrogen absorption and desorption kinetics for nano-MgH_2 with and without the metal oxides under the same conditions, which are at 300 °C under 8.4 bar hydrogen pressure for the absorption reaction, and at 300 °C in vacuum for the desorption reaction. They indicated that the Mg with Cr_2O_3 sample has the fastest hydrogen absorption rate among all the oxide catalysts, and the most rapid hydrogen desorption properties were revealed for the MgH_2 with V_2O_5 and Fe_3O_4 samples [27]. Barkhordarian *et al.* investigated the properties of 0.2 mol% Nb_2O_5 catalyzed MgH_2 and compared the kinetic properties for Mg-H system without catalyst at 250 and 300 °C. Nb_2O_5 has even more active properties as the catalyst than the previous reports [28]. Among the metal and oxide catalysts reported so far, it is recognized that Nb_2O_5 is the best catalyst for absorption and desorption.

In fact, Hanada *et al.* reported that a remarkable improvement of H_2 absorption

kinetics was observed by preheating of the mechanically milled MgH_2 with 1 mol% Nb_2O_5, which possesses mesoporous of 32 Å size, and the catalyzed Mg was able to absorb 4 wt.% of hydrogen even at room temperature under lower pressure than 1 MPa within 10 secwith a final capacity reached to more than 5 wt.% [29]. Considering this result, it is expected that the activation energy of the absorption reaction, $E_{abs}(H_2)$, is decreased to small enough value. Although the hydrogen absorption for Mg are generally performed at higher temperature than 300 °C [24, 30, 31], such high temperature is not necessary for the Mg catalyzed by Nb_2O_5.

The chemical state of Nb_2O_5 added to Mg was reported by Hanada *et al*. [32] and Friedrichs *et al*. [33]. Hanada *et al*. performed the X-ray absorption spectroscopy to characterize the chemical state of 1 mol% oxides (mesoporous Nb_2O_5, V_2O_5, TiO_2^{nano}) on Mg. The results indicated that the chemical state of transition metal oxides had been changed during ball milling. The three catalysts after ball milling were nearly corresponding to NbO, VO, and Ti_2O_3, respectively [32], indicating that these states are catalytic active. Moreover, the variation of nano-Nb_2O_5 added to Mg during hydrogen absorption and desorption reactions of the Mg were investigated by in situ XANES and XRD analyses under isothermal (300 °C) condition by Friedrichs *et al*. They concluded that the Mg-Nb-O ternary phase was generated, and the phase acted to the pathway of H diffusion [33].

References

[1] NEDO. 2013; Available from: http://www.nedo.go.jp/news/press/AA5_100201.html.

[2] NIST. Available from: http://webbook.nist.gov/chemistry/.

[3] JHFC. 2009; Available from: http://www.jari.or.jp/Portals/0/jhfc/data/pdf/fcv.pdf.

[4] L. Kawasaki Hevy Industries. 2005; Available from: http://www.khi.co.jp/knews/backnumber/bn_2005/pdf/news138_05.pdf.

[5] N. L. Rosi, J. Eckert, M. Eddaoudi, D. T. Vodak, J. Kim, M. O'Keeffe and O. M. Yaghi: *Science*. 300 (2003) 1127-1129.

[6] L. Schlapbach, *Hydrogen in Intermetallic Compounds I*. Vol. 63. 1993, Springer-Verlag.

[7] Y. Fukai, *The Metal-Hydrogen System*. 1993, Springer-Verlag.

[8] Y. Fukai, K. Tanaka and H. Uchida, *Hydrogen and metals, in Japanese*. 2 nd ed. 2002, Uchida Roukakuho publishing CO., LTD.

[9] L. Schlapbach, *Hydrogen in Intermetallic Compounds II*. Vol. 67. 1992, Springer-Verlag.

[10] H. Y. Leng, T. Ichikawa, S. Hino, N. Hanada, S. Isobe and H. Fujii: *J. Power Sources*. 156 (2006) 166-170.

[11] A. Züttel, P. Wenger, S. Rentsch, P. Sudan, P. Mauron and C. Emmenegger: *J. Power Sources*. 118 (2003) 1-7.

[12] Y. Kojima, H. Miyaoka, T. Ichikawa and S. L. Suib, *Chapter 5 - Hydrogen Storage Materials*. 2013, Elsevier.

[13] T. Yoshida, *Corpus of technologies for hydrogen, in Japanese*. 2003, NTS.

[14] T. V. Choudhary, C. Sivadinarayana and D. W. Goodman: *Catal. Lett.* 72 (2001) 197-201.

[15] S. F. Yin, B. Q. Xu, X. P. Zhou and C. T. Au: *Applied Catalysis A: General*. 277 (2004) 1-9.

[16] Y. Kojima, K. Tange, S. Hino, S. Isobe, M. Tsubota, K. Nakamura, M. Nakatake, H. Miyaoka, H. Yamamoto and T. Ichikawa: *J. Mater. Res*. 24 (2009) 2185-2190.

[17] H. Yamamoto, H. Miyaoka, S. Hino, H. Nakanishi, T. Ichikawa and Y. Kojima: *Int. J. Hydrogen Energy*. 34 (2009) 9760-9764.

[18] J. J. Reilly Jr and R. H. Wiswall Jr: *Inorg. Chem.* 6 (1967) 2220-2223.

[19] J. J. Reilly and R. H. Wiswall: *Inorg. Chem.* 7 (1968) 2254-2256.

[20]   J. F. Stampfer, C. E. Holley and J. F. Suttle: *J. Am. Chem. Soc.* 82 (1960) 3504-3508.

[21]   J. J. Vajo, S. L. Skeith and F. Mertens: *The Journal of Physical Chemistry B*. 109 (2005) 3719-3722.

[22]   B. Vigeholm, K. Jensen, B. Larsen and A. S. Pedersen: *Journal of the Less Common Metals*. 131 (1987) 133-141.

[23]   A. Zaluska, L. Zaluski and J. O. Ström–Olsen: *J. Alloys Compd.* 288 (1999) 217-225.

[24]   J. Huot, G. Liang, S. Boily, A. Van Neste and R. Schulz: *J. Alloys Compd.* 293-295 (1999) 495-500.

[25]   G. Liang, J. Huot, S. Boily, A. Van Neste and R. Schulz: *J. Alloys Compd.* 292 (1999) 247-252.

[26]   N. Hanada, T. Ichikawa and H. Fujii: *J. Phys. Chem. B*. 109 (2005) 7188-7194.

[27]   W. Oelerich, T. Klassen and R. Bormann: *J. Alloys Compd.* 315 (2001) 237-242.

[28]   G. Barkhordarian, T. Klassen and R. Bormann: *Scr. Mater.* 49 (2003) 213-217.

[29]   N. Hanada, T. Ichikawa, S. Hino and H. Fujii: *J. Alloys Compd.* 420 (2006) 46-49.

[30]   J. F. Fernández and C. R. Sánchez *J. Alloys Compd.* 340 (2002) 189-198.

[31]   R. K. Singh, T. Sadhasivam, G. I. Sheeja, P. Singh and O. N. Srivastava: *Int. J. Hydrogen Energy*. 38 (2013) 6221-6225.

[32]   N. Hanada, T. Ichikawa, S. Isobe, T. Nakagawa, K. Tokoyoda, T. Honma, H. Fujii and Y. Kojima: *J. Phy. C.* 113 (2009) 13450-13455.

[33]   O. Friedrichs, D. Martínez-Martínez, G. Guilera, J. C. S. López and A. Fernández: *J. Phys. Chem. C*. 111 (2007) 10700-10706.

2. **Purpose of this thesis**

To realize Mg for practical use as a hydrogen storage material, kinetic improvement is the most important issue. So far, it is reported that the kinetics properties are improved by ball milling and addition of catalysts. Although the transition metals possessing d-electron are considered as conventional catalysts for dissociation of gaseous molecules such as H_2, it is noteworthy that some oxide shows excellent catalytic effects for the Mg-H system as mentioned in section 1.5 of previous chapter. Regarding the catalysis of oxide, it is expected that the mechanism is different from that of conventional metal catalysts, however details of the catalytic effects have not been clarified yet.

In this thesis, the catalytic effects of oxides for hydrogenation and dehydrogenation reactions of Mg are investigated from the kinetic and thermodynamic points of view. Particularly, the kinetic properties of Mg-H system catalyzed by Nb_2O_5, which is the most effective catalyst among the oxides reported so far, are examined in further detail, and the chemical states during the reactions are *in-situ* studied by using X-ray absorption spectroscopy in detail to understand the catalytic mechanism.

3. Experimental procedures

3.1 Sample

3.1.1 Materials

MgH$_2$ powder with particle size of several microns was purchased from Alfa Aesar. The purity is 98 wt.%, and the remaining phase- Mg is present as an impurity. As catalysts, zirconium oxide (ZrO$_2$, 99 % purity, powder) and niobium oxide (Nb$_2$O$_5$,99.5 % purity, powder with 32 Å mesoporous) were purchased from Alfa Aesar and Sigma-Aldrich, respectively. As the reference materials used for X-ray absorption spectroscopy, niobium (Nb, 99.96 % purity, powder) and niobium oxide (NbO, 99.7 %, powder) were purchased from Rare Metallic.

3.1.2 Mechanical ball milling method

All the samples were prepared by mechanical ball milling method. The starting material i.e. MgH$_2$ with or without catalyst were weighed in the batches of 100, 200, or 300 mg as the total amount and put into a Cr steel pot (30 cm^3 in volume) with 20 balls made from steel (7 mm in diameter) or ZrO$_2$ (8 mm in diameter). The experimental conditions are listed in Table 3-1 and 3-2. The milling pot was specially designed for the mechanical milling which is equipped with a Swagelok quick connector for evacuating the pot and introducing gases such as hydrogen, and the process was performed in the Sieverts' type apparatus shown in Fig. 3-1. The mixed samples were mechanically milled under 1.0 MPa of hydrogen gas (> 99.9999%) for 20 h with 370 rpm by a planetary ball-milling apparatus (Fritsch P7) as shown in Fig. 3-2. The samples were always handled in the glove-box filled with high purity Ar gas (>

99.9999%) to prevent the oxidation of samples.

3.1.3 Hydrogenation and dehydrogenation treatments

The dehydrogenated samples were obtained by heat treatment of the milled samples under vacuum condition for 12 h. The temperature conditions of the samples in section 4.1 were set as equals to the peak temperatures obtained by the thermal decomposition mass spectroscopy (TDMS), which are later shown in Fig. 4-1-1 in the next chapter. For the other samples used for investigation of the Nb_2O_5 catalytic effect, the temperature was chosen to be 220 °C and 330 °C for the catalyzed MgH_2 and the milled MgH_2 without catalysts, respectively. Hereafter, the dehydrogenated samples are denoted as c-Mg and m-Mg, respectively.

The hydrogenated samples were derived from above dehydrogenated samples. The hydrogenation treatments of c-Mg and m-Mg were performed at 220 °C and 330 °C under 1.0MPa of H_2 for 12h, respectively. The obtained samples are denoted as c-MgH_2 and m-MgH_2, respectively.

Table 3-1 Milling conditions of the samples for the section 4-1

Materials	total amount (mg)	kind of balls
MgH_2	100	ZrO_2
MgH_2	200	ZrO_2
MgH_2	300	ZrO_2
MgH_2	100	Steel
MgH_2+ZrO_2	100	Steel

Table 3-2 Milling conditions of the samples which are the precursors of m-Mg and c-Mg

Materials	total amount(mg)	kind of balls
MgH_2	300	Steel
$MgH_2+Nb_2O_5$	300	Steel
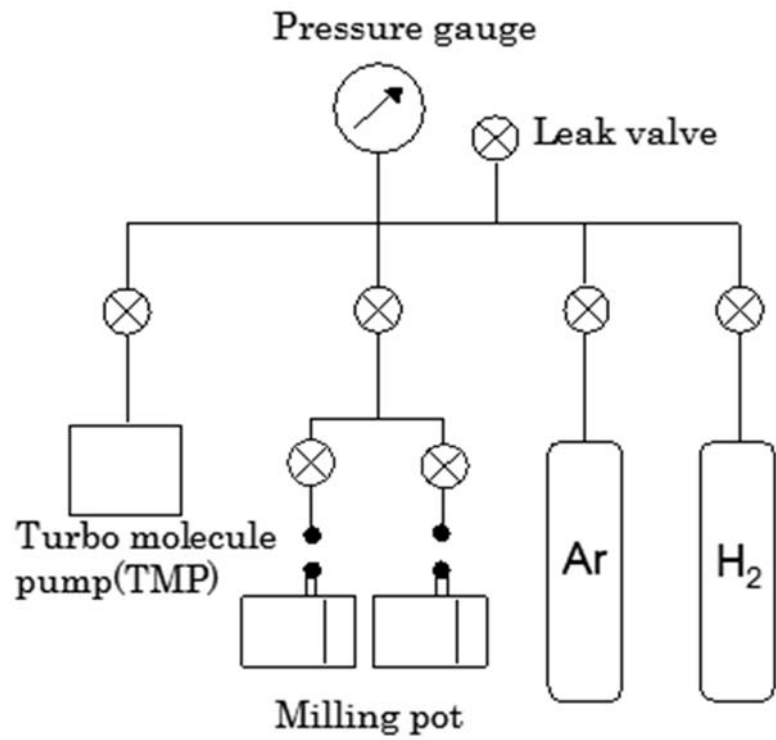
Figure 3-1 Sievert-type equipment
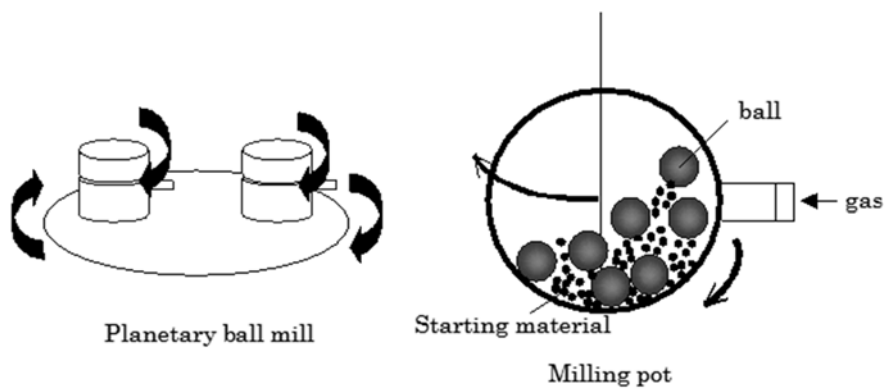
Figure 3-2 Planetary ball mill and milling pot

3.2   Characterization techniques

3.2.1 Thermogravimetry (TG) and thermal desorption mass spectroscopy (TDMS) analysis

(1) Measurement Principle

Thermogravimetry (TG) and thermal desorption mass spectroscopy (TDMS) are used to investigate the thermal properties of samples. The weight loss during heating process is measured by TG. In the case of simple hydrogen storage materials like metal hydrides, the desorbed gas is only hydrogen, therefore the amount of hydrogen can be estimated from the weight loss. TDMS is able to identify the desorbed gas by mass analysis. The mass spectroscopy is constituted from the three parts, which are an ionization source, a quadruple mass spectrometer, and a detector, as shown in Fig. 3-3 [1]. A turbo molecular pump (TMP) is used to maintain ultra-high vacuum in the TDMS chamber.

At first, the gas molecules desorbed from the sample are ionized by conflicting electron beam in the ionization part. After that, the ions are separated according to their mass number, m, and electrical charge, z, in the quadruple mass spectrometer. Fig. 3-4 shows the scheme of a quadruple electrode which is constituted from two couples of electrodes [2]. Regarding the electrodes, the modulated voltage, $U+V\cos\omega t$, are applied, where U and $V\cos\omega t$ are direct current voltage and high frequency voltage, respectively. The only ions which possess the specific ratio between m and z shown as follows, can reach the detector.

$$\frac{m}{z} = \frac{1}{7.22} \cdot \frac{V}{r_0^2 \cdot f^2} \qquad \left[f = \frac{\omega}{2\pi} \right], \qquad (3\text{-}1)$$

where r_0 is the incircle radius surrounded by the quadruple electrodes. Therefore, the

molecular ions are divided by continuous change of V. The passed ions are detected by the detector constituted electron doubling tubes, and the mass spectra of gases desorbed from the samples are obtained.

(2) Measurement procedure

The hydrogen desorption properties in heating process were examined by TG (TG8120, Rigaku Corp.) and TDMS (M-QA200TS, Canon Anelva Corp.). The TG / TDMS experiments were performed for temperature up to 450 ºC with several heating rates i.e. 1, 5, 10, and 20 ºC /min. High-purity He gas (purity > 99.9999 %) was used for flow condition during measurement. In our system, TG and TDMS are connected to each other, therefore both analyses are simultaneously performed. The specially designed apparatuses installed in a glove-box filled with high-purity Ar gas (purity > 99.9999 %) enable us to observe the thermal decomposition reaction by TDMS and TG without exposing the samples to air.

(3) Kinetic analysis

The kinetic properties for hydrogen desorption process are analyzed using the Kissinger equation because this reaction is activated by heat and generally called as "heat activation process".

The reaction rate, v, of the MgH_2 decomposition is expressed by the concentration of MgH_2, ρ, and described as follows,

$$v = -\frac{d\rho}{dt} = K\rho, \tag{3-2}$$

where, K is the kinetic constant. Here, the temperature in the heating process with constant rate is described as follows,

$$T = T_0 + \beta t, \tag{3-3}$$

where T_0, β, and t are the initial temperature, the heating rate, and the reaction time, respectively. When the equation (3-3) is differentiated with respect to t and T, we obtain the following equation,

$$\frac{1}{dt} = \frac{\beta}{dT}. \tag{3-4}$$

From the equations (3-4) substituted by (3-2), the following equation is obtained,

$$\frac{d\rho}{dT} = -\frac{K\rho}{\beta}, \tag{3-5}$$

The Arrhenius equation is expressed as,

$$K = K_0 \exp\left(-\frac{E}{RT}\right), \tag{3-6}$$

On substituting eqn. (3-6) for (3-5), the following equation is obtained,

$$\frac{d\rho}{dT} = -\frac{K_0 \rho}{\beta} \exp\left(-\frac{E_d}{RT}\right), \tag{3-7}$$

where E, K_0, and E_d are the activation energy, the frequency factor, and the activation energy of hydrogen desorption reaction, respectively. The peak temperature can be represented by following relation:

$$\frac{d^2\rho}{dT_P^2} = 0, \tag{3-8}$$

Hence, the following equation is derived by differentiation of the equation (3-7),

$$\frac{d\rho}{dT_p} = -\frac{\rho}{RT_P^2} E_d. \tag{3-9}$$

Therefore, the following equation is derived by the equations (3-7) and (3-9),

$$\ln\frac{\beta}{T_P^2} = -\frac{E_d}{RT_P} + \ln\left(\frac{RK_0}{E_d}\right). \tag{3-10}$$

This equation indicates that the K_0 and E_d can be estimated by using the relation between β and T_p.
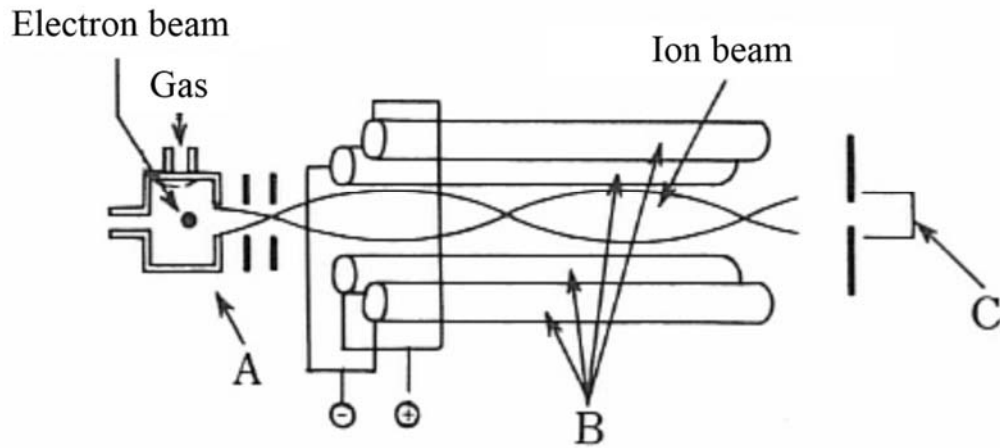
Figure 3-3 The interior scheme of TDMS apparatus A: ionization source, B: quadruple mass spectrometer, and C: detector [1]
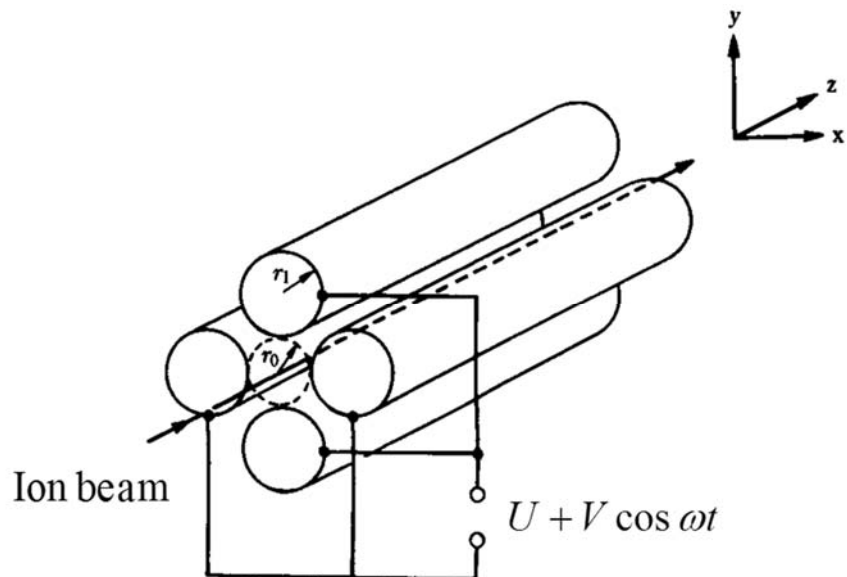
Figure 3-4 Quadruple mass spectrometer [2]

3.2.2 Inductively Coupled Plasma Atomic Emission Spectroscopy (ICP-AES) analysis

(1) Measurement Principle

Inductively coupled plasma atomic emission spectroscopy (ICP-AES) is used for the element analysis, and the apparatus consists of two parts which are a plasma generator and detector. The element ratio of the sample can be estimated by the analysis of the atomic emission spectra caused by the elements included in the sample. The sample solution is introduced to the plasma. Fig. 3-5 shows the mechanism for the emission of the light. The atoms present in the sample reach to excited state E_2 from the ground state E_0 by absorbing thermal energy from the surrounding plasma. This excitation of atoms generates light of specific wavelength based on the difference of the energy level between E_2 and E_0. The generated light is dispersed and detected by the detector part. By analyzing the wavelength, the elements are qualitatively and quantitatively identified.

(2) Measurement procedure

The milled samples mentioned in the table 3-1, were dissolved into the nitric acid solutions, and the solutions were introduced to the ICP-AES apparatus (Shimadzu Corp.). The plasma was generated from high-purity Ar gas. The generated lights were dispersed by the Echelle diffraction grating and detected by the charge-coupled device.
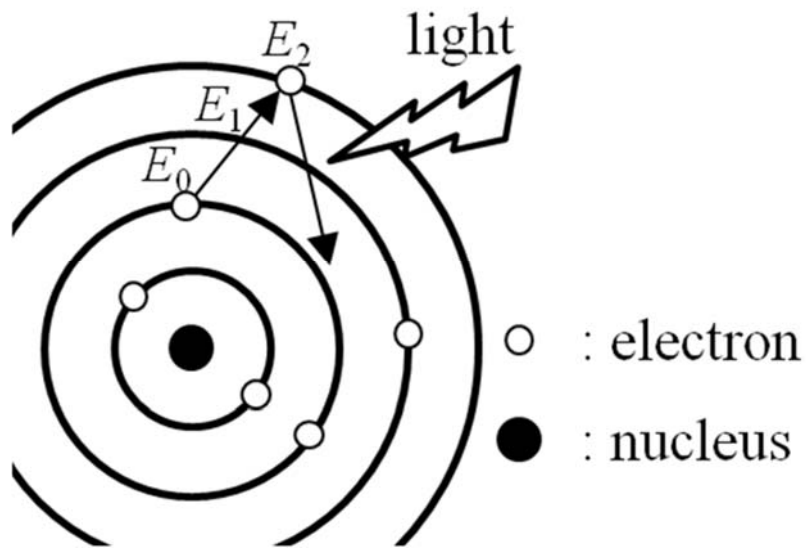
Figure 3-5 Mechanism for emission of light

3.2.3 Sievert's type apparatus

(1) Measurement Principle

The Sievert's type apparatus is able to estimate the amount of hydrogen reacted with metals by measuring the gaseous pressure and temperature. The apparatus scheme is shown in Fig. 3-6. The volume of system is measured in advance. In order to perform measurement, the reservoir tank is first filled with a certain amount of hydrogen then valve V3, which connects the tank and reactor cell, is opened. The amount of gaseous hydrogen is continuously estimated from the pressure variation.

(2) Kinetics property

To examine the kinetics of hydrogen absorption of the Mg samples, which were prepared by ball milling and heat treatment, the amounts of absorbed hydrogen and deuterium were measured as a function of reaction time under several conditions. The experimental conditions i.e. the initial hydrogen pressure and temperature were chosen as according to the properties of each sample and are listed in the table 3-3. A 100 mg sample was transferred into the reactor cell and this reactor cell is then connected to the rest of the system using quick connector. In order to start the measurement hydrogen was introduced in the reservoir part by keeping valve V3 closed. After that, valve V3 was opened, and the pressure variation was monitored. The amount of absorbed hydrogen was estimated from the pressure changes all the time during measurement by using the special software (SUZUKI SHOKAN Co., Ltd.). The final hydrogen amount was checked and corrected by TG measurement after the experiments. The kinetics measurement should be under isothermal condition, however, the hydrogen absorption for Mg is an exothermic reaction which could enhance the reactor temperature during

the measurement. Therefore, the initial pressure and reactor temperature denoted as Temp. 2, were set in such a way that it can keep the reaction rate as slow as possible.

(3) Thermodynamic property

Pressure-Concentration-Isotherms (PCIs) experiments were performed for m-Mg and c-Mg. The equilibrium pressures and the amount of hydrogen were obtained under isothermal condition with variation of the hydrogen pressure step by step. The waiting time for stabilization of each pressure was 2 h, and the experimental temperatures were 250, 300, and 350 °C. The obtained isotherm was calibrated by using the result of blank measurement at each temperature and the software (SUZUKI SHOKAN Co., Ltd.).
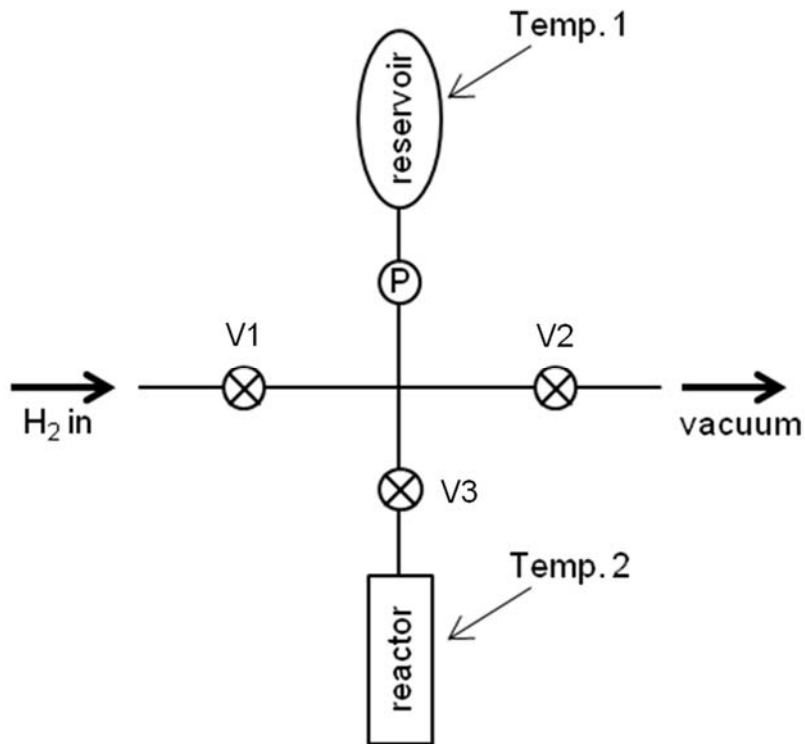
Figure 3-6 Sievert's type apparatus scheme

Table 3-3 Combinations of each experimental condition for measuring the hydrogen absorption rate

sample	initial pressure (MPa)	temperature range (°C)	result figure
dehydrogenated samples after ball milled with ZrO_2 balls	1.0	room temperature	Fig. 4-1-3
c-Mg	1.0	RT ~ 250 °C	Fig. 4-3-6
c-Mg	0.2	−50 ~ −10 °C	Fig. 4-3-9, 4-3-14
m-Mg	2.0	60 ~ 100 °C	Fig. 4-3-12

3.2.4 Powder X-ray diffraction (XRD) measurement

(1) Measurement Principle

Powder X-ray diffraction is an important method to identify the crystal structure and to determine the lattice parameters. The principle scheme of X-ray diffraction is shown in Fig. 3-7 [3]. The incident X-ray, which is denoted as 1 in Fig. 3-7, is reflected on the lattice planes expressed by the Miller indices (hkl), where the distance between lattice planes is same (hkl) and denoted as d_{hkl}. When the reflected X-ray from the second lattice plane, which is shown as 2, interferes with the beam reflected from the first plane, the X-ray diffraction occurs. As shown in Fig. 3-7, the optical path difference between 1 and 2 is estimated as $2d_{hkl}(\sin\theta)$. The constructive interference will only be occurredonly if following condition is satisfied,

$$n\lambda = 2d_{hkl}(\sin\theta), \tag{3-11}$$

where n and λ are an integer number and the wavelength of the X-ray respectively. This diffraction condition is known as Bragg's law, and the XRD pattern, which reflects the crystal structure, is obtained by changing the incident angle of the X-ray.

The relation between the half width of the peak and crystalline size is well known as Scherrer's equation shown as follows,

$$D = \frac{K\lambda}{\beta\cos\theta} \tag{3-12}$$

where, D, K, λ, β, and θ are the crystalline diameter, the Scherrer constant, the wavelength of X-ray, the half width of the peak, and the diffraction angle of the peak, respectively. This equation indicates that the half width inversely correlates with the crystalline size.

(2) Measurement procedure

In this work, powder XRD (RINT 2000, Rigaku Corp.) was used to identify the phases of sample. The X-ray source was Cu-$K\alpha$ (λ=1.54 Å), and the output energy was 8 kW (40 kV, 200 mA). The sample was spread and adhered on the glass plate with a high vacuum grease (Apiezon® Grease, M&I Material Ltd.) as a glue. The sample was covered with a polyimide sheet (8 μm thickness, Kapton®, Du Pont-Toray Co., Ltd.) to avoid the oxidation of the samples. The obtained XRD patterns were analyzed by using the software (Jade 5.0 and PDXL) and powder diffraction files. The crystalline sizes of the samples were compared each other by the half widths estimated from the main peak of each spectrum.
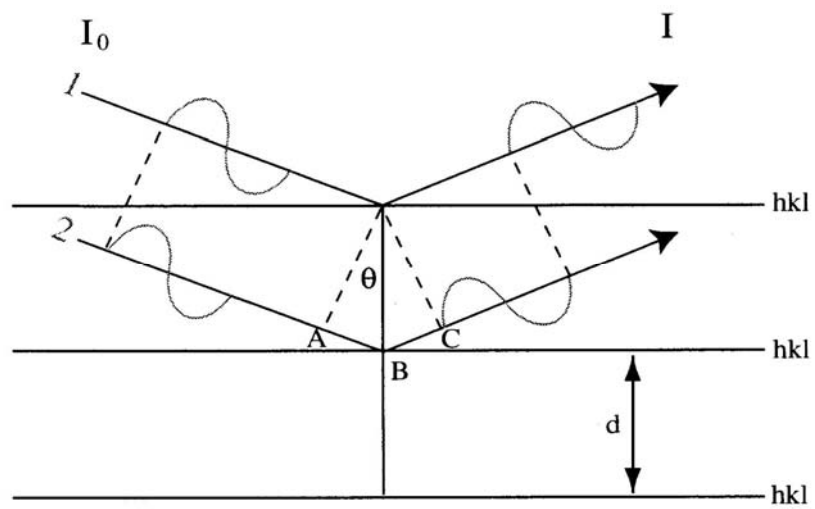
Figure 3-7 Diffraction of X-rays from planes in a crystal [3]

3.2.5 X-ray absorption spectroscopy (XAS) measurement

(1) Measurement principle

X-ray absorption spectroscopy (XAS) is used for characterizing the chemical state (electronic structure) and the local atomic environment of target element. When the X-ray with the energy, E, and intensity, I_0, permeates through the sample with the thickness, t, the intensity of the transmitted X-ray, I, is described as follows,

$$I = \exp(-\mu t)I_0 \text{,}$$
(3-13)

where μ is an absorption coefficient. When the energy of X-ray corresponds to the transition energy between the two kinds of energy states, the electrons at lower state should be excited by receiving energy from X-ray, consequently, the X-ray absorption phenomenon is observed. The typical XAS spectrum is shown in Fig. 3-8(a) [4]. It is noticed that the μ tends to decrease with increasing E. However, several drastic increases of μ are observed at specific energy which is corresponding to the X-ray absorbed by the excitation of electrons as mentioned above. This energy point is called as absorption edge, and the energy is particular for the target element. The structure around the absorption edge is called as X-ray absorption near-edge structure (XANES) shown in Fig. 3-8(b), and tail of the edge is called as extended X-ray absorption fine structure (EXAFS) [4]. The XANES is reflected by the chemical state of the target element in the samples. Although it is generally discussed that the spectrum is simply affected by the valence of the elements, strictly speaking, the spectrum shape is related to the density of state in conduction band due to the crystal structure of the sample. In the EXAFS range, the oscillation originated in the local structure such as a coordination state of target elements is shown. Here, XANES and EXAFS are collectively called as X-ray absorption fine structure (XAFS). Thus, the XAS is a useful tool to characterize

the chemical state and local atomic environment of the catalyst. In XANES region, the chemical state of the target element can be examined by the chemical shift of the absorption edge and the shape of spectrum. EXAFS profile reflect the bonding length and the coordinated atoms in particular; each bonding length can be estimated by the curve fitting with a radial distribution function, which is obtained by Fourier transformation.

(2) Measurement procedure

The XAFS derived from niobium (Nb) in the catalyzed MgH_2, c-Mg, c-MgH_2, and the references, which are Nb, NbO, and Nb_2O_5, were measured by XAS for the K-edge of Nb at BL28XU, which is a beam-line of SPring-8 synchrotron radiation facility in Japan. The samples were formed into pellets with 1cm diameter by 600 kg of pressure. For measuring the in situ XAS during the hydrogenation and dehydrogenation reactions, a special environmental cell capable to control the hydrogen pressure, was used. For the absorption measurement for c-Mg, the hydrogen pressure was controlled from 0 to 0.2 MPa at room temperature, and finally, the atmosphere was exchanged to Ar gas. For the desorption process, c-MgH_2 was used as the starting sample, and the temperature was controlled from room temperature to 210 °C with Ar flow condition. After that, the temperature was returned to room temperature. In order to analyze the XAFS, a software, REX2000 (Rigaku Corp.), was used.
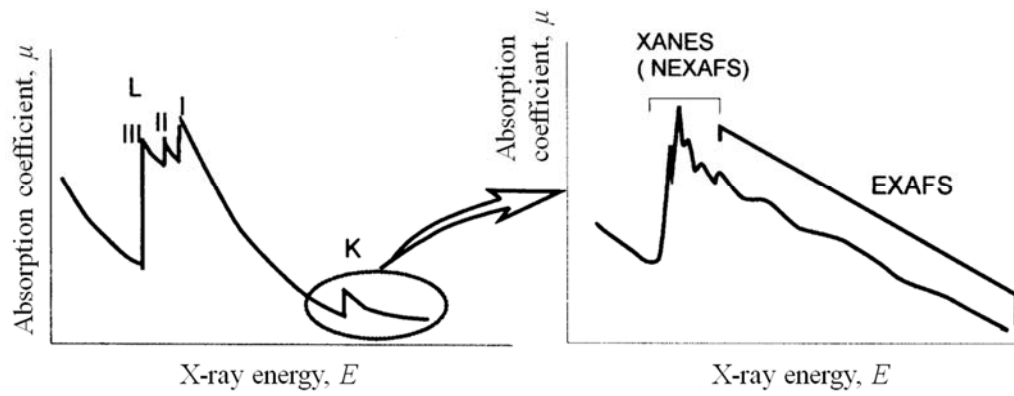
(a)   (b)

Figure 3-8 (a) X-ray absorption spectrum (b) X-ray absorption spectrum near K-edge
[4]

References

[1]   S. Tanaka and Y. Iida, *Instrumental Analysis, in Japanese*. 3 rd ed. 1997, Shokabo.

[2]   S. Kinoshita，T. Matsushita，M. Tanaka，T. Yamaguchi and M. Fujiwara, *Instrumental Analytical Chemistry, in Japanese*. 1988, Sankyou publishing company.

[3]   I. Nakai and F. Izumi, *Powder X-ray Diffraction Analysis, in Japanese*. 2002, Asakura Shoten.

[4]   T. Ohta, *X-ray absorption spectroscopy, in Japanese*. 2002, IPC.

4. Results and Discussion

4.1 ZrO$_2$

Fig. 4-1-1 (A) and (B) show the TDMS spectra corresponding to desorbed hydrogen from the samples prepared in the various conditions. It is found that the peak temperatures for hydrogen desorption of the MgH$_2$ milled with ZrO$_2$ balls are lowered with the decrease in the sample quantities from 300 to 100 mg. The sample prepared by milling 100 mg of MgH$_2$ with ZrO$_2$ balls has the lowest hydrogen desorption peak at around 240 °C. It is 115 °C lower than that of MgH$_2$ milled with steel balls shown as (B)-d, and the peak corresponding to as−received MgH$_2$ is at 408 °C. Moreover, the sample prepared by milling 100 mg of MgH$_2$ and 1mol% ZrO$_2$ with steel balls showed a hydrogen desorption peak at 239 °C in Fig. 4-1-1 (B)-e. It is almost the same as the 100 mg of MgH$_2$ milled with ZrO$_2$ balls. This result implies that these two samples has similar constitutions, namely ZrO$_2$ should be doped into MgH$_2$ from ZrO$_2$ balls during the ball milling and improved the kinetics of hydrogen desorption.

The amount of ZrO$_2$ for each sample has been determined by ICP-AES measurement as Zr cation in nitric acid solution. The obtained values are 0.72, 0.15, and 0.079 mol% for the samples prepared by milling 100, 200, and 300 mg of MgH$_2$ with ZrO$_2$ balls, respectively. The relationship between Zr content and H$_2$ desorption temperature is shown in Fig. 4-1-2. It is revealing that the hydrogen desorption temperature of MgH$_2$ can be effectively reduced by increasing the Zr amount. The above results indicate that the milling with ZrO$_2$ balls results in addition of ZrO$_2$ into the MgH$_2$, and the mingled ZrO$_2$ spices has a catalytic effect for hydrogen desorption reaction of MgH$_2$.

For the hydrogen absorption reaction, the properties of the samples were measured at room temperature under 1.0 MPa H_2 pressure by the Sieverts' type apparatus, and the results are shown in Fig. 4-1-3. The sample milled with steel balls was not able to absorb H_2 at room temperature. On the other hand, the samples milled with ZrO_2 balls were able to absorb hydrogen even at room temperature within 5 h. The hydrogen absorption amount is found to be 3.6, 2.7, and 1.5 wt.% for the sample prepared by milling 100, 200, and 300 mg of MgH_2, respectively. From the above results, it is noticed that the containing ZrO_2 significantly improved the hydrogen absorption kinetics of magnesium, even though the ZrO_2 content is as low as < 0.1 mol%.

Fig. 4-1-4 (a) shows the XRD patterns of the as-milled MgH_2 samples. ZrO_2 phase is not able to be detected in all the samples. These results should be owing to the low concentration or being amorphous. Only β-MgH_2 phase is found in the sample milled with steel balls, whereas a very weak diffraction peaks corresponding to γ-MgH_2, which is a metastable structure of MgH_2, are also found in the XRD patterns of the samples milled with ZrO_2 balls. These results indicate that the ZrO_2 mingled from the balls changed the milling condition to the more effective one.

Above results reveal that the ZrO_2 balls have the effects to improve kinetics of for the both hydrogen absorption and desorption reactions of Mg that is lacked for the steel balls. The effects of mingled ZrO_2 are summarized as follows: ZrO_2 possesses the catalytic effects to Mg-H system, and enhances the milling effect to MgH_2 as forming a metastable phase.
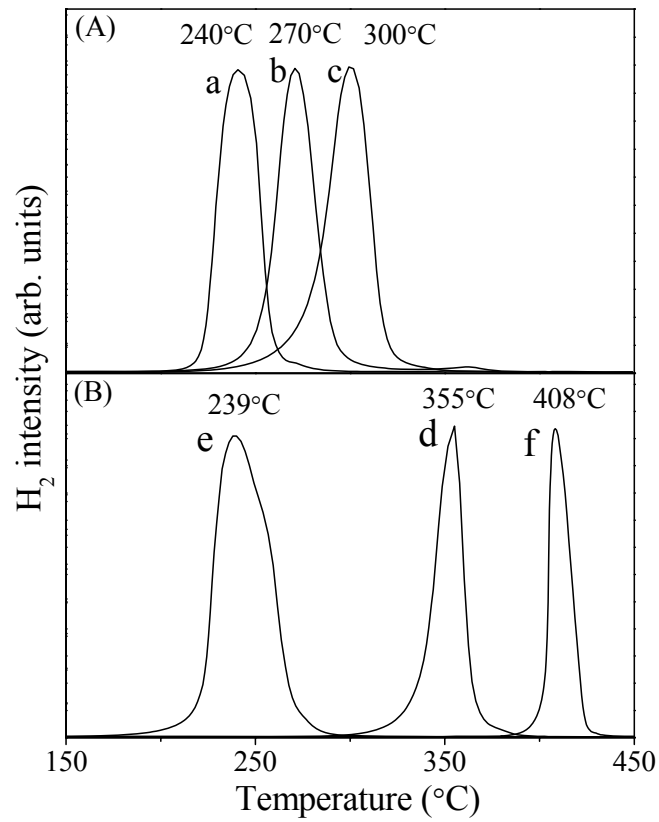
Figures 4-1-1 (A) TDMS results corresponding to H_2 for the (a) 100, (b) 200, (c) 300 mg MgH_2 milled with ZrO_2 balls, and (B) TDMS results of H_2 for the (d) 100 mg MgH_2, (e) 100 mg MgH_2 + 1 mol% ZrO_2 milled with steel balls, and (f) as-received MgH_2.
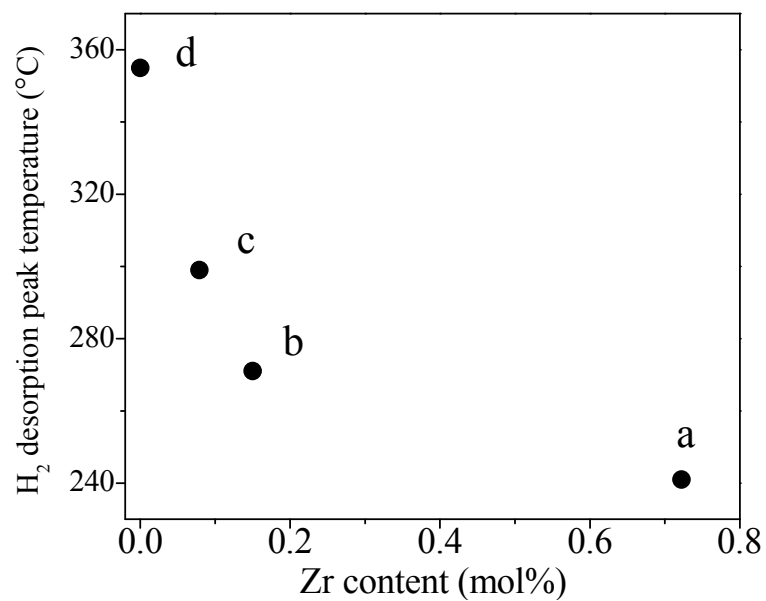
Fig. 4-1-2 Relationship between Zr content and H_2 desorption temperature for the (a) 100, (b) 200, (c) 300 mg MgH_2 milled with ZrO_2 balls, and the (d) 100 mg MgH_2 milled with steel balls.
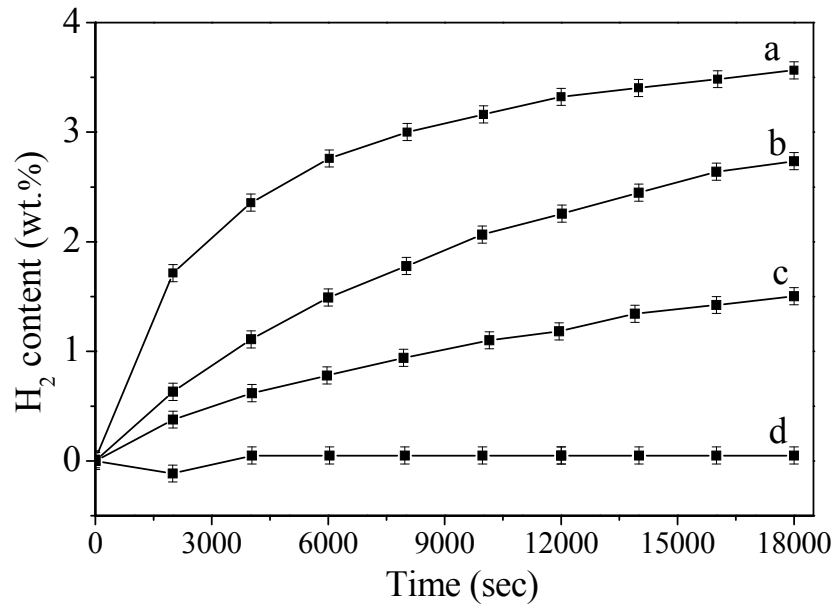
Fig. 4-1-3 Isothermal hydrogen absorption profiles of the complete dehydrogenated samples of (a) 100, (b) 200, (c) 300 mg MgH_2 milled with ZrO_2 balls, and (d) 100 mg MgH_2 milled with steel balls at room temperature under hydrogen pressure of 1MPa within 5 hours.
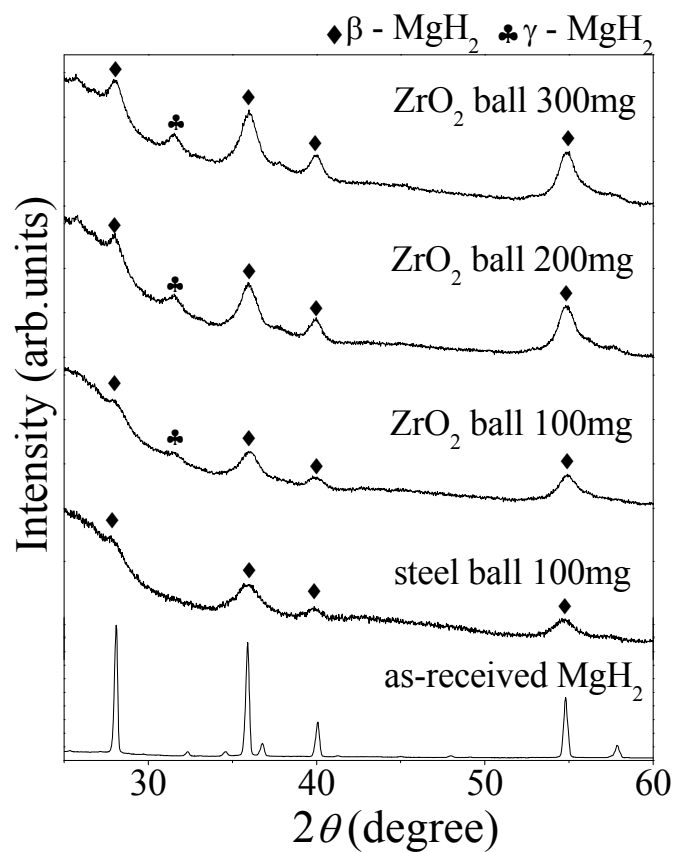
Figures 4-1-4 XRD patterns of the 100, 200, 300 mg MgH₂ milled with ZrO₂ balls, the 100 mg MgH₂ milled with steel balls, and as-received MgH₂.

4.2   Nb$_2$O$_5$

It has been reported that Nb$_2$O$_5$ is the most effective catalyst for Mg-H system [1]. The hydrogen absorption and desorption properties of Mg catalyzed with Nb$_2$O$_5$ was investigated by Hanada *et al*. Regarding the absorption properties, 4 wt.% of hydrogen can be absorbed to the Mg within 10 seconds under 1.0 MPa of H$_2$ pressure at room temperature. And the activation energy for dehydrogenation of MgH$_2$ catalyzed with Nb$_2$O$_5$ was estimated as 71 kJ/mol [2].

This chapter is constructed from two purposes which are in order to understand "the effect of Nb$_2$O$_5$ on the kinetic property" and "the catalytic mechanism of Nb$_2$O$_5$". For the high dispersion of Nb$_2$O$_5$ on Mg surface, the ball milling was performed. In the sections from 4.2.1 to 4.2.3, in order to investigate the effect of Nb$_2$O$_5$, the non-catalyzed Mg was also prepared by ball milling as same condition as the Mg catalyzed with Nb$_2$O$_5$ because the surface of Mg is activated by only ball milling [3], and the kinetic properties of the hydrogenation and dehydrogenation reactions for both samples have been investigated. As mentioned above, it is possible that the milling with the ZrO$_2$ balls enhances the kinetics of hydrogen absorption and desorption of Mg. Thus, the addition of Nb$_2$O$_5$ to MgH$_2$ was performed by using the steel balls. In the section 4.2.4, the catalytic mechanism of Nb$_2$O$_5$ is discussed.

So far, the characterization of Nb$_2$O$_5$ added to Mg was carried out by using XAS measurement for the samples after hydrogenation and dehydrogenation. The X-ray absorption near-edge structure (XANES) spectra of the as-milled, dehydrogenated, and hydrogenated samples are almost same as that of NbO, indicating that the chemical state of Nb$_2$O$_5$ is changed to that of NbO by the mechanochemical reaction during the ball milling process. Furthermore, the XANES spectrum of the dehydrogenated sample is

slightly shifted from the as-milled sample [4]. In this work, the interaction between hydrogen and niobium oxide is discussed in further detail.

4.2.1 Kinetics

Hydrogen desorption reaction

Hydrogen desorption profiles of the pure MgH_2 samples obtained by TDMS are shown in Fig. 4-2-1. The TDMS analyses were performed under He flow condition, and the partial pressure of H_2 was kept below 0.1 MPa, this ensure that the hydrogen desorption is observed under 300 °C thermodynamically. However, the as-milled sample has a peak at about 345 °C, and the reduction of peak temperature is about 10 °C by the heat treatment (rehydrogenation). In general, the heat treatment gives a sintering effect of particles, suggesting that the active sites for hydrogen desorption on the surface should be decreased by decrease in the surface area and reduction of crystal distortion or defects. On the other hand, the hydrogen absorption and desorption treatment is used for activating the surface for conventional alloys. Considering the results, it is implied that the activation of Mg surface by hydrogen absorption and desorption reactions would be prior to the sintering effects, which simultaneously exist.

The TDMS profiles of the Nb_2O_5 catalyzed MgH_2 samples are shown in Fig. 4-2-2. By the catalytic effects for hydrogen desorption, the peak temperature is shifted to 230 °C from 347 °C of the milled MgH_2. Here, the onset temperature of hydrogen desorption for c-MgH_2 is estimated as 150 °C from Fig. 4-2-2. The result indicates that the partial pressure is approximately below 820 Pa, where the equilibrium pressure of MgH_2 is 0.1 MPa at 300 °C. The result suggests that the kinetics of hydrogen desorption reaction of MgH_2 has been improved by addition of Nb_2O_5. Thus, Nb_2O_5

has a significant catalytic effect for hydrogen desorption, and it is better catalyst than ZrO_2 because the peak temperature is at 230 °C, which is lower than MgH_2 with ZrO_2 in Fig. 4-1-1. It is also noteworthy that the heat treatment is also effective for the kinetic improvement because the peak temperature of hydrogen desorption is further reduced by the dehydrogenated and rehydrogenated handlings. For Mg catalyzed with Nb_2O_5, the activation and sintering effects during the hydrogen desorption and absorption cycle as described above should be considered. However, it is found that the kinetic improvement is greater than that of non-catalyzed Mg. These results implies that the dispersed Nb_2O_5 is changed to more effective state during hydrogenation treatments, in other words, it is possible that the metastable state formed by the milling for dispersion on MgH_2 has been changed to homogeneous and active state as catalyst.

In order to investigate the thermal effects, the Nb_2O_5 catalyzed Mg was rehydrogenated at different temperatures. The hydrogen desorption profiles of the rehydrogenated samples are shown in Fig. 4-2-3. Here, the H_2 desorption intensity at −196 °C is magnified ten times. Although the hydrogen desorption profiles were able to be obtained, the results at −196 °C was omitted from the analyses because the intensity was not enough. The peak temperature is found to be lower with a decrease in rehydrogenation temperature except for the as-milled MgH_2 sample without catalyst and heat treatments. Above results indicate that the temperature of rehydrogenation is also important factor for the kinetics of hydrogen desorption reaction in addition to the effects of hydrogen absorption and desorption treatments as mentioned above. It is expected that the reduction of hydrogen desorption temperature by the hydrogenation at low temperature is related to the structural factor, which is the crystalline growth.

To examine the crystalline size of MgH_2, the XRD patterns corresponding to the

rehydrogenated samples shown in Fig. 4-2-4 were analyzed. Here, it was difficult to analyze the sample rehydrogenated at -79 °C because the observed peaks were assigned to only Mg although the small amount of hydrogen desorption was observed. It is noticed that the peaks around 42 ° correspond to MgO phase are visible in all the profiles, indicating that the Mg was oxidized by Nb_2O_5 during ball milling, and the MgO remains even the sample was exposed to hydrogen. The relation among the rehydrogenation temperature, peak temperature, and the half width of MgH_2 has been summarized in Fig. 4-2-5. Here, the values of half width are estimated from the peak at 54.6 ° attributed β phase of MgH_2 by using Scherrer's equation and expressed as opened marks. A rough tendency suggests that the higher rehydrogenation temperature lead to bigger crystalline size and higher peak temperature. For the sample rehydrogenated at room temperature denoted as RT, the value of half width and hydrogen desorption temperature is relatively lower and higher, respectively, in view of the tendency. This result indicates that the reactor temperature was exceeded the setting temperature by the reaction heat during the hydrogenation, thus the crystalline size of RT is same as that of sample rehydrogenated at 200 °C. This phenomenon is also shown in the hydrogen absorption experiments indicated in Fig. 4-2-6 [5]. In general, the reaction rate should be faster at higher temperature condition, however, the results are contrary to the expectation. It can be understood that the hydrogenation was interrupted by the reaction heat, which must have increased the equilibrium pressure of Mg. As a result, the hydrogen absorption reaction was milder in the latter region of the experiment than those at higher temperature conditions. For the samples prepared for the experiment of Fig. 4-2-5, it is expected that the same phenomena has been occurred, suggesting that the crystalline size of RT reached to that of sample

prepared at 200 °C. Regarding the sample prepared at −40°C, the small crystalline size could be preserved because the hydrogenated reaction was gradually progressed. On the other hand, for the as-milled sample, the peak temperature of hydrogen desorption is relatively higher although the crystalline size is smaller than that of sample hydrogenated at −40 °C. This result indicates that activation of the catalyst, which is obtained during hydrogen desorption and absorption cycle, is more important compared with the control of crystalline size. From the above results, the heat treatment for activation of the catalyst and the suppression of crystal growth for MgH_2 by the rehydrogenation at low temperature, which could be realized by catalytic effect of Nb_2O_5, are required to obtain better kinetics for the hydrogen desorption reaction of MgH_2.

To understand the catalytic effect of Nb_2O_5 for hydrogen desorption process, the kinetic parameters such as activation energies, $E_{des}(H_2)$, of the catalyzed and milled MgH_2 denoted as c-MgH_2 m-MgH_2, respectively, are estimated. The H_2 desorption profiles for c-MgH_2 and m-MgH_2 were obtained by TDMS with several heating rates, and the profiles are shown in Fig 4-2-7. All the samples showed similar peak shapes, indicating that each reaction involve the same reaction process. The Kissinger plot is drawn by using the peak temperatures and the heating rates as shown in Fig. 4-2-8 and Fig. 4-2-9, respectively. The $E_{des}(H_2)$ of c-MgH_2 and m-MgH_2 are estimated to be about 70 and 129 kJ/mol, respectively. The $E_{des}(H_2)$ of c-MgH_2 is close to the standard enthalpy of MgH_2, −74 kJ/mol [6]. Thus this indicates that the surface barrier is decreased by the catalytic effect. Considering the activation energy of H diffusion in Mg, which was reported as 40 kJ/mol [7], the $E_{des}(H_2)$ of m-MgH_2 is attributed to other step such as the recombination of hydrogen atoms on the Mg surface.

From above results, it is clarified that the reaction rate of dehydrogenation is clearly improved by the addition of 1 mol% Nb_2O_5 into MgH_2. As a result, the activation energy for the hydrogen desorption is reduced to almost zero because its value, 70 kJ/mol, is close to ΔH. Moreover, the crystalline size of MgH_2 is an important factor for the reaction. The small crystalline size is preserved by the hydrogenation under low temperature condition. In addition, the dehydrogenation and rehydrogenation processes have further improvement effect for the dehydrogenation rate, indicating that the dispersed Nb_2O_5 is changed to more homogeneous and active state as catalyst during these processes.
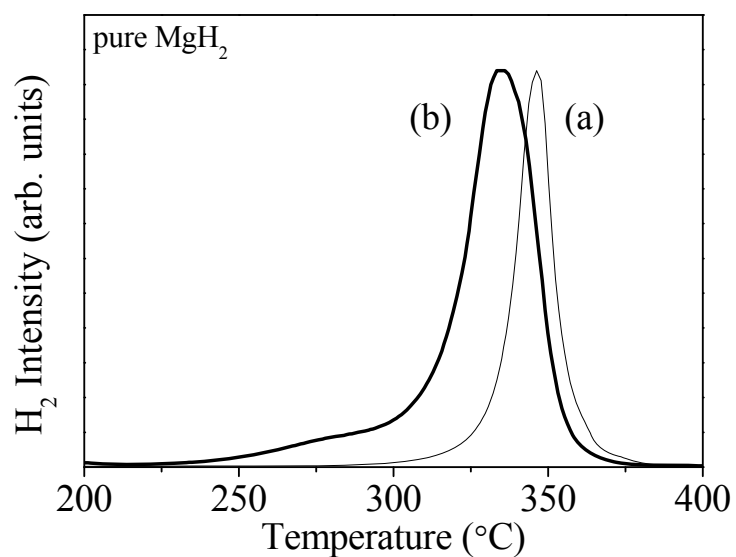
Figure 4-2-1 The TDMS (H₂) profile of the pure MgH$_2$ obtained (a) as ball milled sample and (b) after dehydrogenation and rehydrogenation handling of (a) sample.
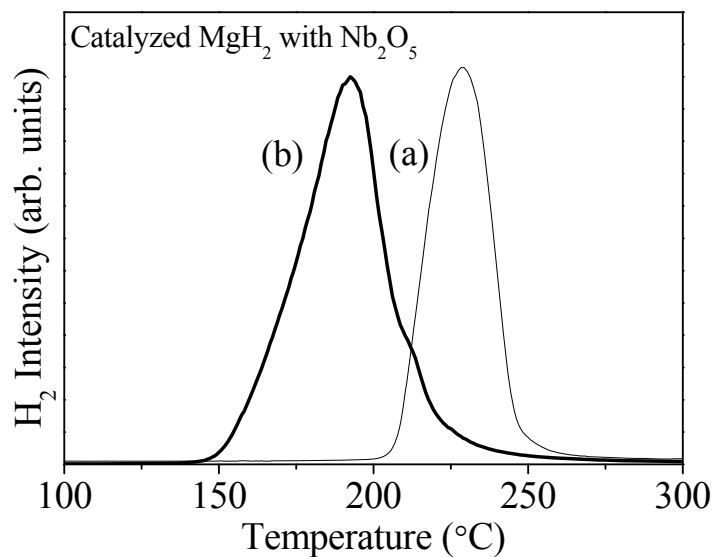
Figure 4-2-2 The TDMS (H₂) profile of the MgH$_2$ catalyzed with Nb$_2$O$_5$ obtained (a) as ball milled sample and (b) after dehydrogenation and rehydrogenation handling of (a) sample.
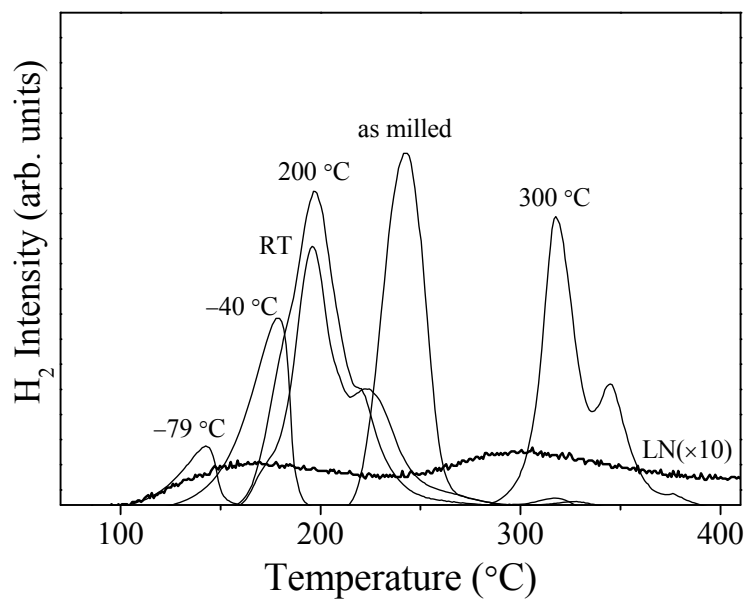
Figure 4-2-3 The TDMS (H$_2$) profile of the MgH$_2$ catalyzed with Nb$_2$O$_5$ samples obtained after ball milled and rehydrogenation handling at several temperature conditions: −79, −40, RT (room temperature), 200, and 300 °C, respectively. Here, the profile of LN (-196 °C) is shown as ten times larger intensity than the obtained intensity.
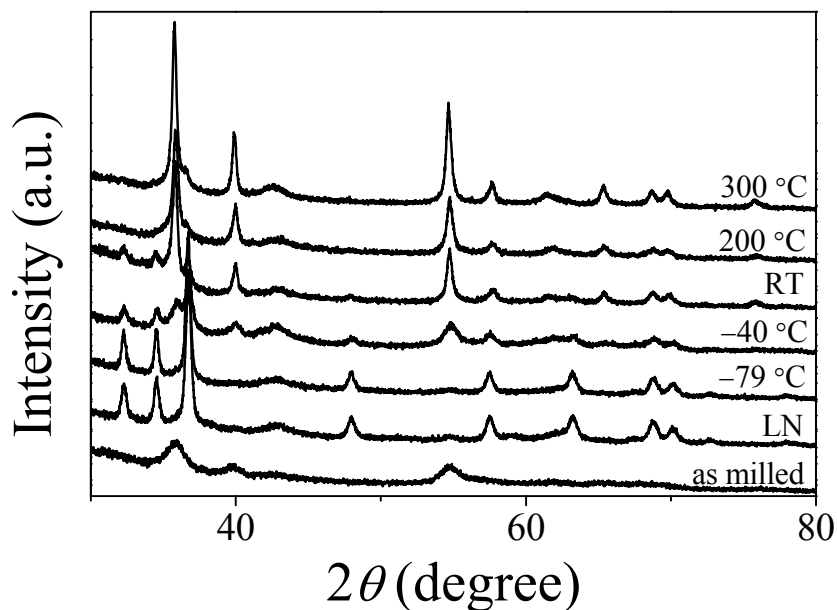
Figure 4-2-4 XRD patterns of the MgH_2 catalyzed with Nb_2O_5 samples after rehydrogenation at each temperature.
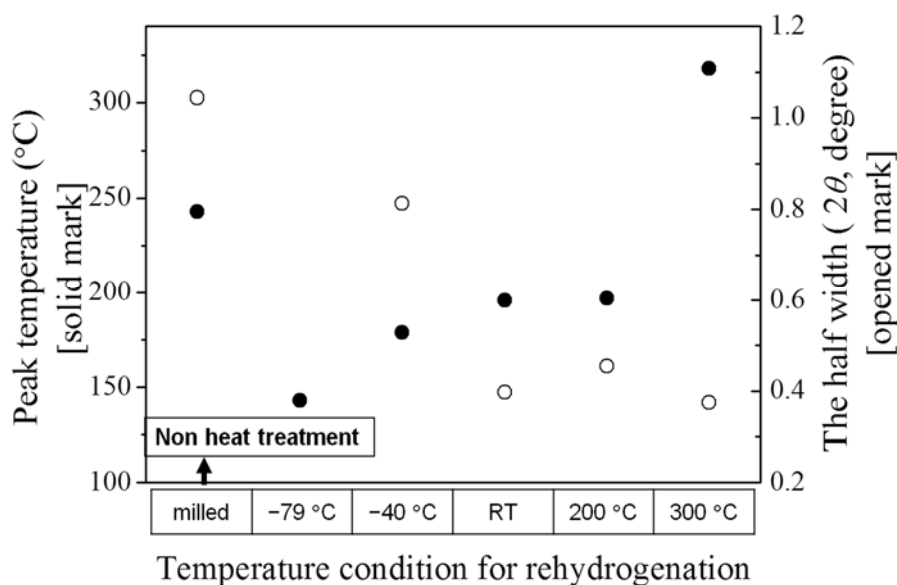
Figure 4-2-5 The relation among the rehydrogenationated temperature, the H_2 peak temperature in TDMS (solid marks), and the half width of the peak at 54.6 ° in XRD profiles (opened marks) of the MgH_2 catalyzed with Nb_2O_5 samples obtained after the rehydrogenation.

70
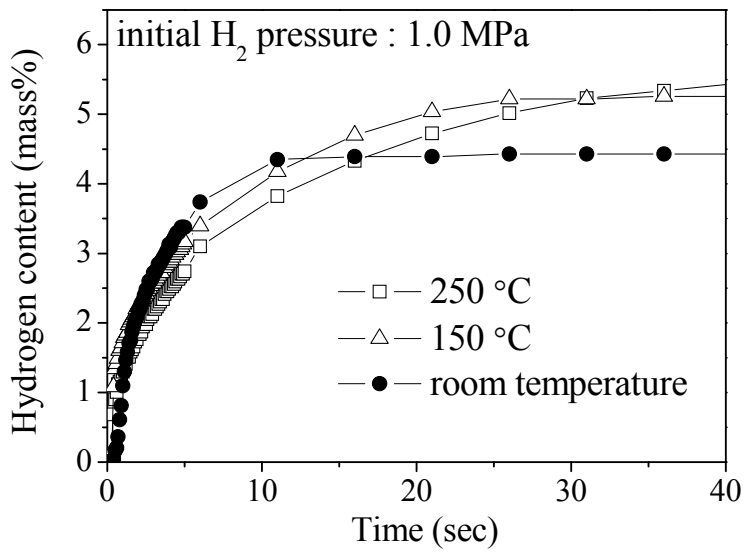
Figure 4-2-6 H_2 absorption curves of Mg catalyzed with Nb_2O_5 as a function of time under

1.0 MPa H_2 at 250 (□), 150 °C (△), and room temperature (●) [5].
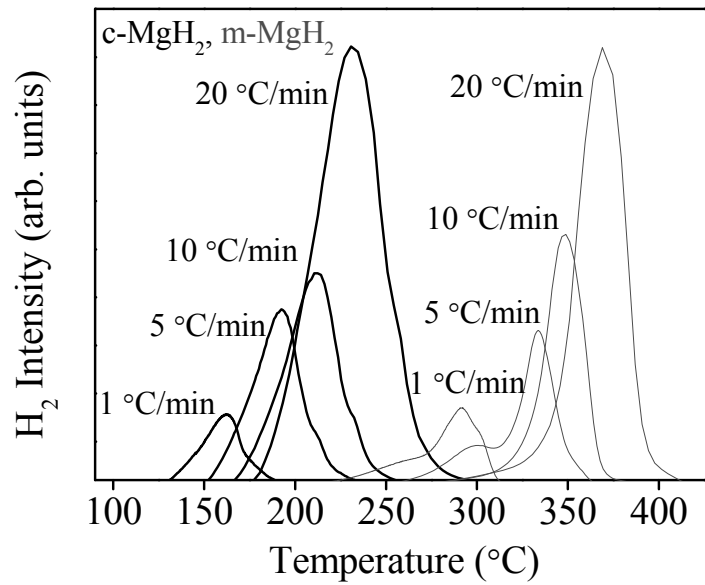
Figure 4-2-7 H_2 desorption profiles of MgH_2 catalyzed with Nb_2O_5 (black line) and m-MgH_2 (gray line) with different heating rate, 1, 5, 10, and 20 °C/min.
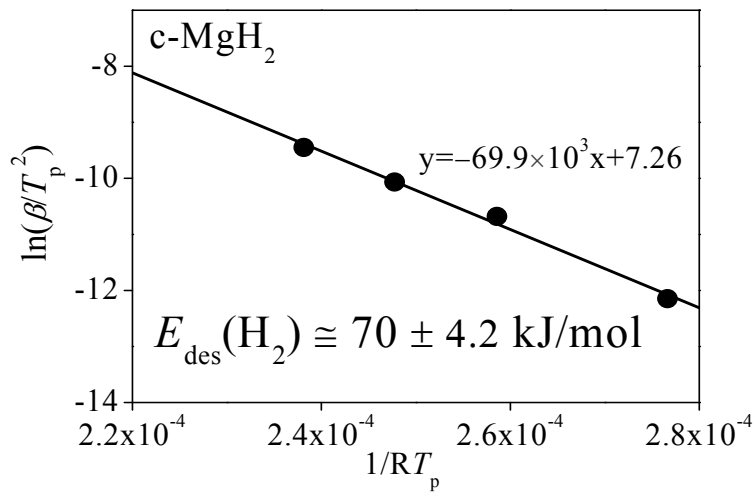
Figure 4-2-8 Kissinger plots on the peak temperature of hydrogen desorption profiles and heating rate for the MgH_2 catalyzed with Nb_2O_5.
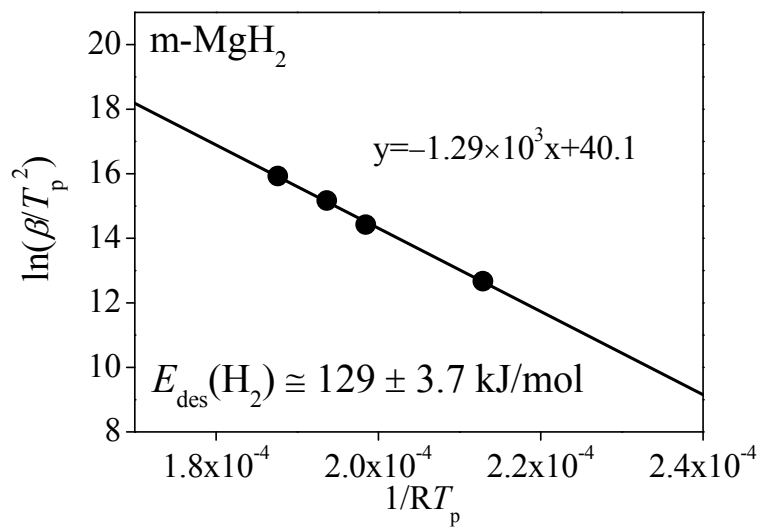
Figure 4-2-9 Kissinger plots on the peak temperature of hydrogen desorption profiles and heating rate for the ball milled MgH_2

Hydrogen absorption reaction

For the investigation of essential kinetics of the hydrogen absorption reaction of Mg, the suppression of the heat generation is found necessary as discussed in above section. Hence, the hydrogen absorption experiments are performed under lower pressure and temperature. In the reaction conditions, the reaction rate becomes lower, suggesting that the essential analyses of kinetics can be achieved because of suppression of the exothermic effect. Here, this experimental condition has been realized for the Nb_2O_5 catalyzed Mg with the excellent kinetics on surface reaction.

The hydrogen absorption curves for c-Mg at different temperature are shown in Fig. 4-2-10. It is noteworthy that c-Mg absorbed more than 2 wt.% of H_2 even at -50 °C for 8 h, and the reaction rate is fast enough for analyses. The hydrogen absorption amount has been increased with the temperature elevation. From the initial slope of H_2 absorption profile, the kinetic constant, $K(H_2)$, at each temperature are obtained. The Arrhenius plot of the $K(H_2)$ is shown in Fig. 4-2-11. The activation energy on the H_2 absorption process, $E_{abs}(H_2)$, for c-Mg has been evaluated to be 38 kJ/mol. The $E_{abs}(H_2)$ for various types of catalyzed Mg have been reported so far, and the values from representative literatures are listed in the table 4-2-1. Here, these results are obtained by the similar volumetric method although the experimental conditions such as temperature and H_2 pressure are different. Singh *et al.* demonstrated about the effect of CeO_2 nano-particles as catalyst at 280-320 °C, and reported the estimated activation energy of hydrogen absorption for Mg as 84 kJ/mol [8]. Denis *et al.* reported the effects of metallic nano-particles (Cu, Ni, and Pd) in the temperature range of 200-300 °C, and the estimated activation energy has been reported as 40-70 kJ/mol, respectively [9]. Kojima *et al.* measured the absorption rate for Mg nano-composite material with nano-

Ni/Al$_2$O$_3$/C at 20-200 °C, and then the activation energy has been estimated to be 50 kJ/mol [10]. Yu *et al.* evaluated the kinetics of Mg with 20 mass% alloys samples at 29-93 °C with a reduced activation energy to 27.74 kJ/mol [11]. The value obtained for the c-Mg in this work, 38 kJ/mol, is close to that of well activated Mg reported by Denis *et al.* and Yu *et al.* However, the experimental temperatures are different in all these studies, so it is essentially difficult to directly compare these values, as the rate-determining step for hydrogen absorption could be changed by temperature range.

The hydrogen absorption curves for m-Mg are shown in Fig. 4-2-12. In the case of m-Mg, the experiments are performed in the temperature region from 60 to 100 °C, which is higher than that of c-Mg because the surface is not active for dissociation of H$_2$. Namely, the heat-activation was necessary to analyze the H$_2$ absorption curves. It is noticed that the amounts of absorbed hydrogen for 1 h are almost same as the ones of c-Mg although the conditions are more superior on the kinetics than those of c-Mg. The activation energy of hydrogen absorption for m-Mg has been estimated to be 61 kJ/mol as shown in Fig. 4-2-13. Fernandez *et al.* estimated the activation energy as 90±10 kJ/mol for pure Mg (45 μm particle size) sample under 0.5-2.1 MPa H$_2$ at 300-400 °C [12]. Kojima *et al.* measured activation energy of the ball-milled Mg as 86 kJ/mol, which was synthesized under 9 MPa H$_2$ at 100-200 °C[10]. Our result suggest slightly lower values of activation energy than the above mentioned values. It can be suggestedthat the activation for the surface of m-Mg by the ball-milling in this work is more than those reported before.

From the activation energy of hydrogen absorption and desorption for Mg with and without Nb$_2$O$_5$ obtained in this work, a schematic potential energy diagram about the reaction between hydrogen and Mg as shown in Fig. 4-2-14 can be proposed. The

dotted line indicates the potential energy for the Mg without Nb_2O_5, and the solid line is that for catalyzed with Nb_2O_5. The difference between the activation energy of hydrogen desorption for m-MgH_2, 129 kJ/mol, and that of hydrogen absorption for m-Mg, 61 kJ/mol, is 68 kJ/mol, and this value is almost same as the standard enthalpy change of MgH_2, −74 kJ/mol [6]. This indicates that the both reactions are progressed through the same reaction process, and the rate-determining step is surface reaction. On the other hand, the activation energy of hydrogen desorption reaction for c-MgH_2 is 70 kJ/mol and is close to the standard enthalpy change, indicating that the surface barrier, which is due to the inactive surface against hydrogen molecules, is disappeared by the addition of Nb_2O_5. And if the reaction path of hydrogen absorption is same as hydrogen desorption process, the peculiar behavior, which is the hydrogen absorption reaction of Mg at −50 °C, is comprehensible. The activation energy of hydrogen diffusion in Mg was reported as 40 kJ/mol [7]. The activation energy of hydrogen absorption for c-Mg is found to be 38 kJ/mol, which is almost the same as of the reported activation energy on diffusion process. Therefore, it is expected that the addition of Nb_2O_5 changes the rate-determining step from the surface reaction, which is attributed to dissociate hydrogen molecules, to hydrogen diffusion process. From the above results, it is concluded that the reaction kinetics of Mg has been dramatically improved by the addition of Nb_2O_5, and the hydrogen absorption at −50 °C could be realized.

The activation energy on the H_2 absorption process for c-Mg has been accurately evaluated as 38 kJ/mol. Here, in our previous study, it has been clarified that about 4 wt.% of hydrogen could be absorbed within only 10 sec drastically in the case of 1 MPa of H_2 pressure at room temperature [13]. The fast hydrogenation was caused by the reaction heat to form MgH_2 under high H_2 pressure. Therefore, the accurate

analyses of kinetics in this work were able to be carried out by the low temperature condition realized by Nb_2O_5 catalyst and the low pressure condition to prevent the activation effect of heat by the hydrogenation.

Table 4-2-1 Activation energy of hydrogen absorption for Mg with various kinds of catalysts under each condition.

Source	Catalyst	Temp. range (°C)	$E_{abs}(H_2)$, (kJ/mol)
Singh *et al*.	CeO_2	280~320	84
Denis *et al*.	Cu, Ni, Pd	200~300	40~70
Kojima *et al*.	nano-Ni/Al_2O_3/C	20~200	50
Yu *et al*.	$Ti_{0.4}Cr_{0.15}Mn_{0.15}V_{0.3}$	29~93	27.74
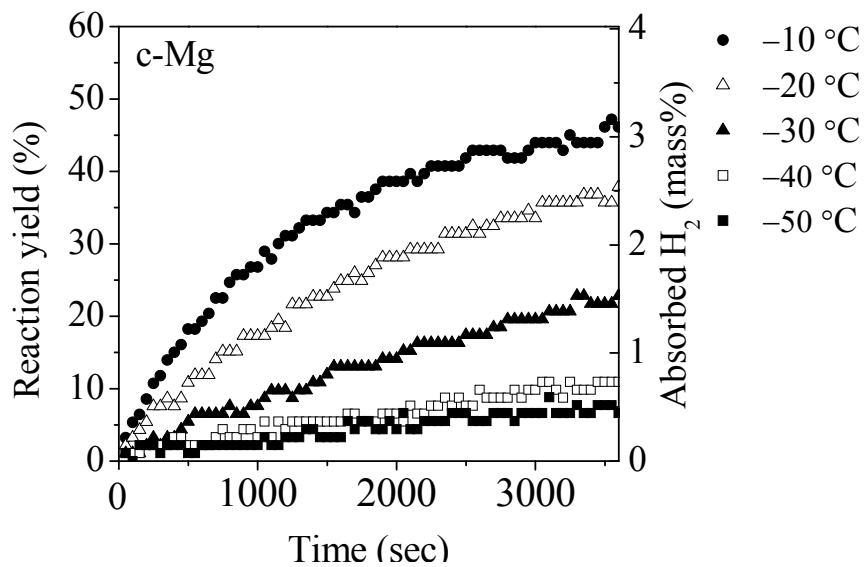
Figure 4-2-10 H_2 absorption curves of Mg catalyzed with Nb_2O_5 (yield of MgH_2) as a function of time under 0.2 MPa of H_2 at $-50(\blacksquare)$, $-40(\square)$, $-30(\blacktriangle)$, $-20(\triangle)$, and $-10(\bullet)$ °C.
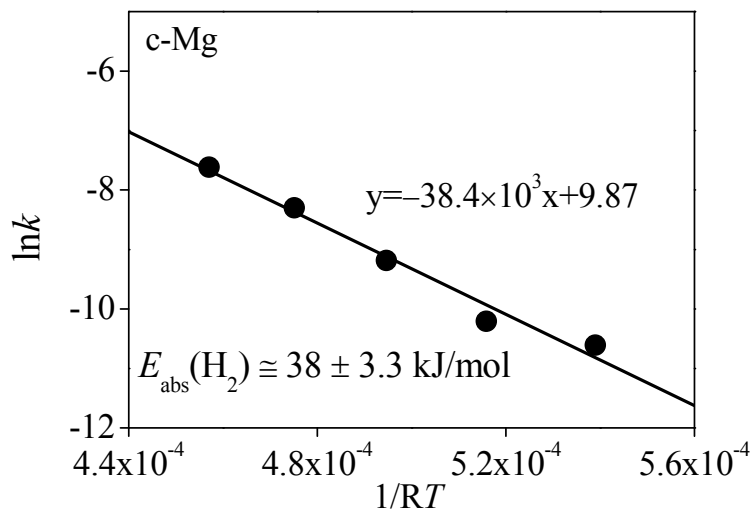
Figure 4-2-11 Arrhenius plots on the initial rate of hydrogen absorption curves as a function of the inverse of each experimental temperature.
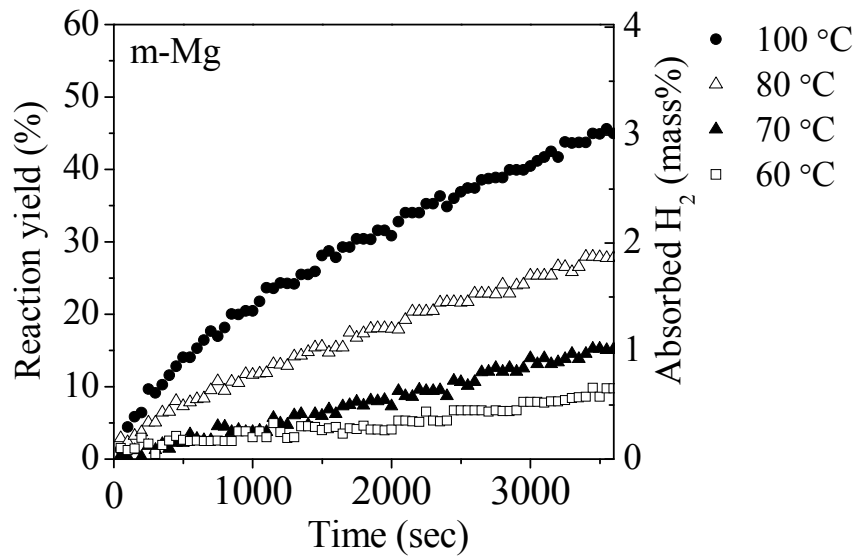
Figure 4-2-12 H_2 absorption curves of ball milled Mg (yield of MgH_2) as a function of time under 2.0 MPa of H_2 at 60($\square$), 70($\blacktriangle$), 80($\triangle$), and 100($\bullet$) °C.
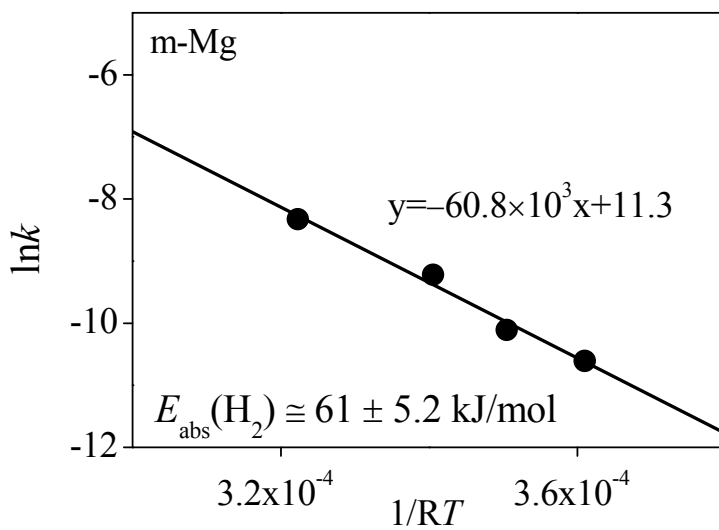
Figure 4-2-13 Arrhenius plots on the initial rate of hydrogen absorption curves as a function of the inverse of each experimental temperature.
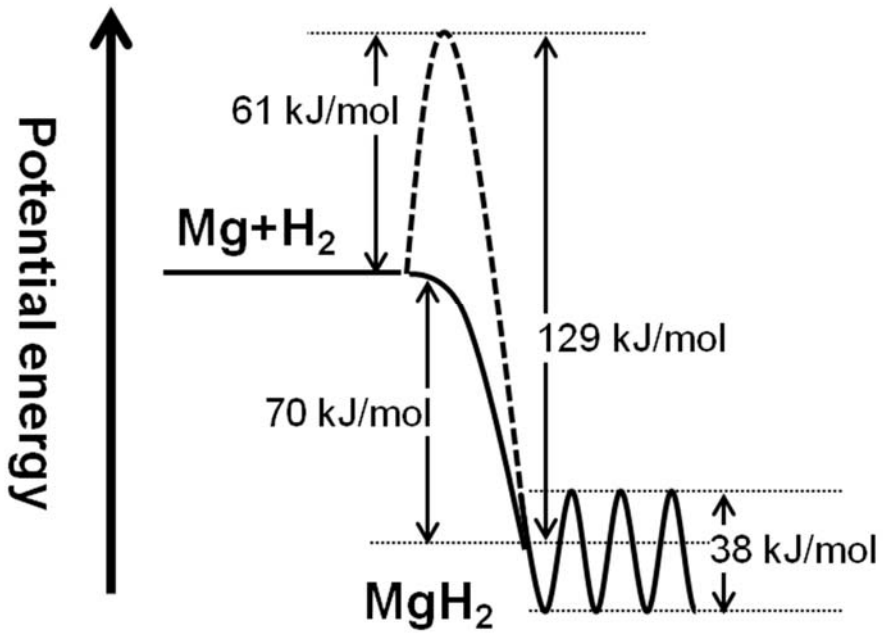
Figure 4-2-14 Schematic potential energy diagram about the reaction between hydrogen and Mg. The dotted line indicates the potential energy of hydrogen and Mg without Nb_2O_5, and the solid line is that of with Nb_2O_5.

4.2.2 Thermodynamics

The reaction kinetics of hydrogen absorption and desorption for Mg are drastically changed by the addition of Nb_2O_5. The alteration of thermodynamic properties is thought to be responsible for this kinetic improvement. In fact, there is a report in the literature which claim this thermodynamical alteration by the formation of a ternary oxide phase composed of Mg, Nb, and O [14]. However, in this work the addition of Nb_2O_5 is only 1 mol%, so it is unlikely for the thermodynamic properties to be altered. But, in order to establish the kinetic improvement strictly, the thermodynamic properties are also investigated.

To investigate the hydrogen capacity, the pressure of the plateau region, and the enthalpy change of the m-Mg and c-Mg, the PCIs measurement have been performed at different temperature conditions. The results of PCI measurements for m-Mg are shown in Fig. 4-2-15. The hydrogen pressure is plotted as a function of hydrogen concentration. It is noticed that about 7 wt.% of hydrogen can be absorbed and desorbed reversibly. In the initial region of absorption and desorption curves especially at 250 °C, bent shapes are observed. Generally, this phenomenon is caused by the potential energy of the hydrogen atoms dissolved in metal. When the hydrogen concentration is gradually changed in the metal, the stability of hydrogen is varied by the continuous variation of surrounding conditions. However, the bent region is longer than that of conventional solid solution, and the flat equilibrium pressures are obtained at higher temperature condition, suggesting that the bent PCI is caused by slow kinetics of m-Mg. From the relations between the experimental temperature and the obtained equilibrium pressure, the van't Hoff plots are performed as shown in Fig. 4-2-16 to estimate the thermodynamic parameters. The ΔH and ΔS of hydrogen desorption

reaction are estimated as 77 kJ/mol H_2 and 138 J/mol K, respectively, and these values are almost same as the database, 74 kJ/mol H_2, and 135 J/mol K [6]

The PCI curves for c-Mg are shown in Fig 4-2-17. The amount of absorbed hydrogen was about 6.3 wt.%, which is about 10% lower than that of m-Mg. The value reached to the theoretical value considering the addition of 1 mol% of Nb_2O_5 (10 wt.%) to Mg. In all plateau regions, the flat equilibrium pressures are obtained in contrast to m-Mg. The van't Hoff plot for the temperatures and the equilibrium pressures are performed as shown in Fig 4-2-18. The ΔH and ΔS have been estimated as 75 kJ/mol H_2 and 136 J/mol K, respectively, and the values are almost same as those of m-Mg. Therefore, the Nb_2O_5 catalyst has no significant effect on the thermodynamic properties although it is effective in kinetic properties which are shown in the initial regions for absorption and desorption especially at 250 °C.
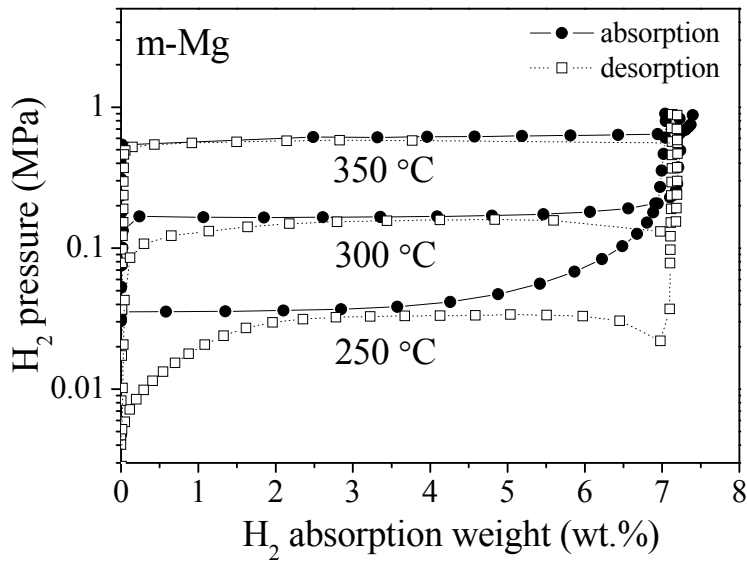
Figure 4-2-15 PCI curves of H₂ absorption and desorption for ball milled Mg at 250, 300, and 350 °C.
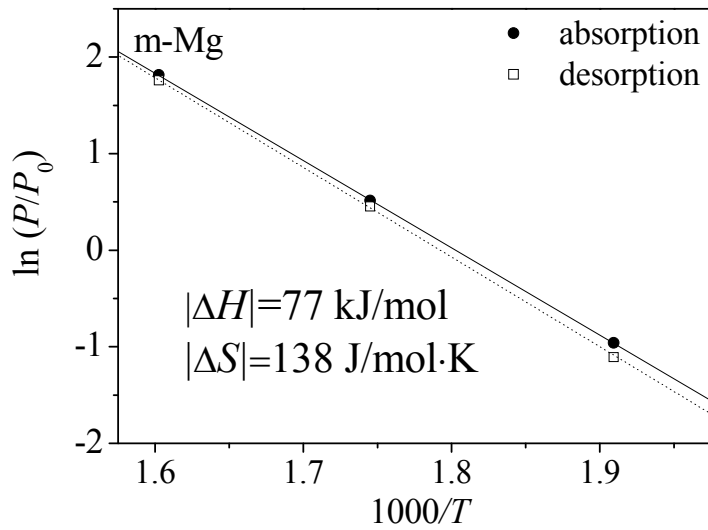
Figure 4-2-16 The van't Hoff plots on the plateau pressure as a function of the inverse of each experimental temperature for the absorption (solid marks) and desorption (open marks) processes.
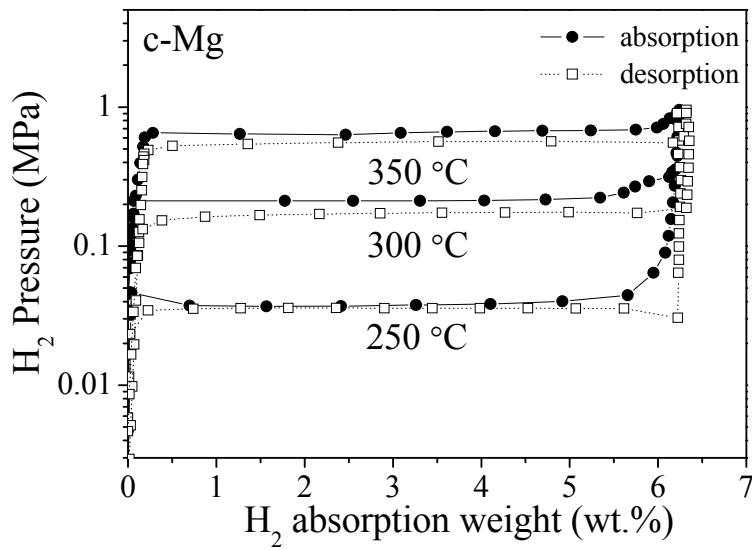
Figure 4-2-17 PCI curves of H2 absorption and desorption for Mg catalyzed with Nb2O5 at 250, 300, and 350 °C.
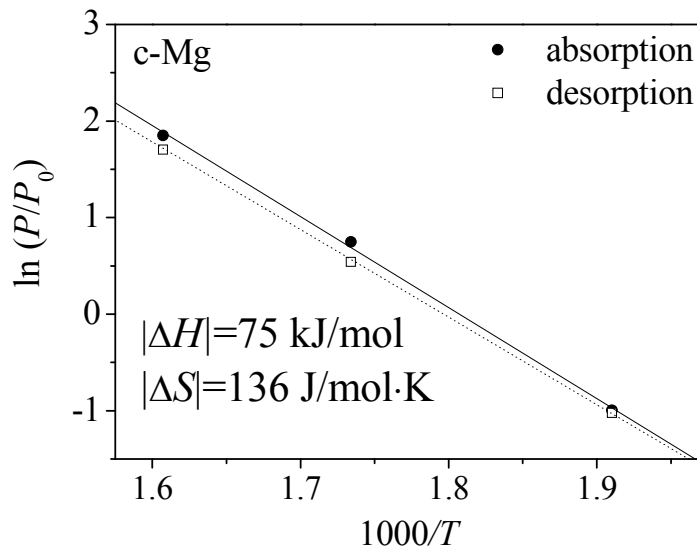
Figure 4-2-18 The van't Hoff plots on the plateau pressure as a function of the inverse of each experimental temperature for the absorption (solid marks) and desorption (open marks) processes.

4.2.3 Isotope effect

Regarding the H_2 absorption reaction for Mg, some papers reported that the rate-determining step is dominated by H diffusion process [12, 15, 16]. These hydrogen absorption experiments were performed to the pristine Mg at enough high temperature condition because the energy was required for decrease in the surface barrier of Mg as mentioned in the chapter 1.5. On the other hand, for Mg catalyzed with Nb_2O_5, it is clear that the barrier became smaller than that of pure Mg by the catalytic effect. If the rate-determining step is attributed to the hydrogen diffusion step, which possesses a sensitive factor for its own mass, the isotope effect should be observed in the kinetics properties by using deuterium instead of hydrogen. The diffusion coefficient of hydrogen in metals such as Ti [17], Fe [18], Y [19], and Ru [20] could be estimated by an isotope effect using deuterium (D). If the hydrogen absorption of Mg is dominated by the diffusion step of hydrogen atoms as described above, the H_2 absorption rate could be affected by the isotope effect, in this case, the rate-determining steps can be identified. The D_2 absorption profiles of c-Mg are shown in Fig. 4-2-19. It is noticed that each initial absorption rate became slower than that of H_2 on the same temperature condition as shown in the inset figure of Fig. 4-2-19. The kinetic constants $K(D_2)$ obtained from the initial slope of D_2 absorption curves are plotted as a function of $1/T$ in Fig. 4-2-20. As the results, $E_{abs}(D_2)$ has been evaluated as 41 kJ/mol. The value is almost same as the one of H_2 absorption in spite of the significant difference between H_2 and D_2 in the absorption curves. Therefore, it is confirmed that the isotopic effect for the kinetic factors such as activation energy is not large enough.

The D_2 desorption profiles for c-MgD_2 are obtained by TDMS with different heating rates as shown in Fig 4-2-21. It is noticed that the peak temperatures at each

86

heating rate are about 10 °C higher than those of H_2 shown in Fig. 4-2-7. From the Kissinger plots, the activation energy of the D_2 desorption process, $E_{des}(D_2)$ has been evaluated as 71 kJ/mol as shown in Fig. 4-2-22. Thus the activation energy has no significant isotopic effect on both the reactions although the reaction rates is clearly different in the hydrogen absorption curves. Thus, it is difficult to discuss the rate-determining steps from the kinetic factors obtained in the experiments. To clearly identify the rate-determining steps of the hydrogen absorption and desorption reactions of Mg, further research from different point of view is necessary.
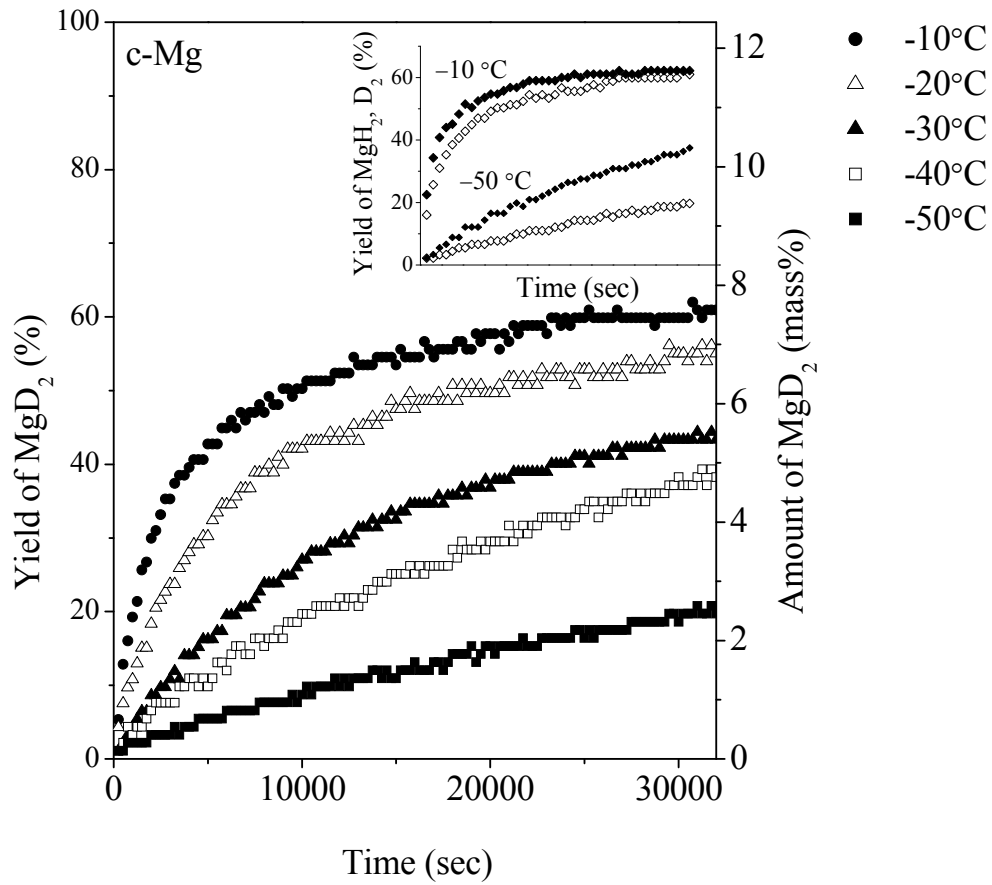
Figure 4-2-19 D$_2$ absorption curves of Mg catalyzed with Nb$_2$O$_5$ (yield of MgD$_2$) as a function of time under 0.2 MPa of D$_2$ at $-50(\blacksquare)$, $-40(\square)$, $-30(\blacktriangle)$, $-20(\triangle)$, and $-10(\bullet)$ °C, and (inset) the comparison of H$_2$ (solid marks) and D$_2$ (open marks) absorption rates for Mg catalyzed with Nb$_2$O$_5$ at -10 and -50 °C.
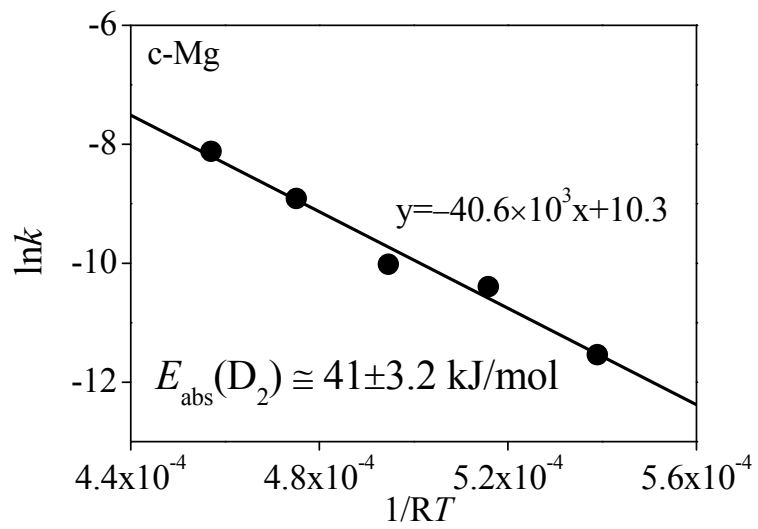
Fig. 4-2-20 Arrhenius plots on the initial rate of deuterium absorption reaction as a function of the inverse of temperature.
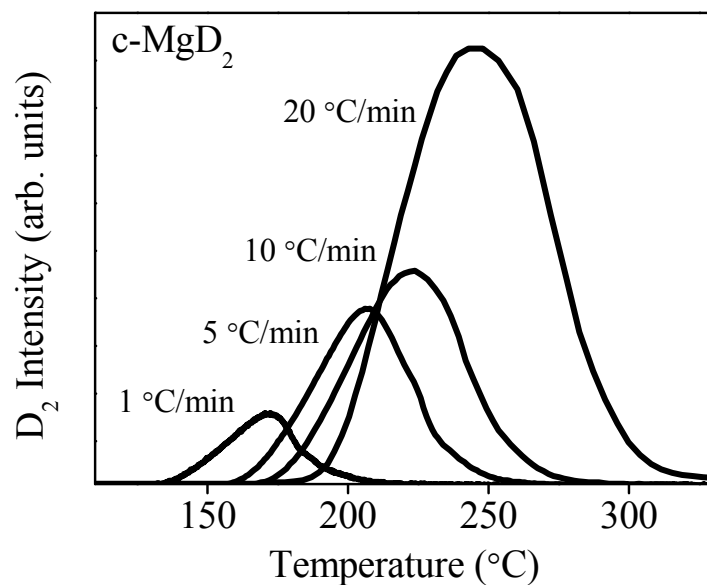
Figure 4-2-21 D_2 desorption profiles of MgD_2 catalyzed with Nb_2O_5 with different heating rate, 1, 5, 10, and 20 °C/min.
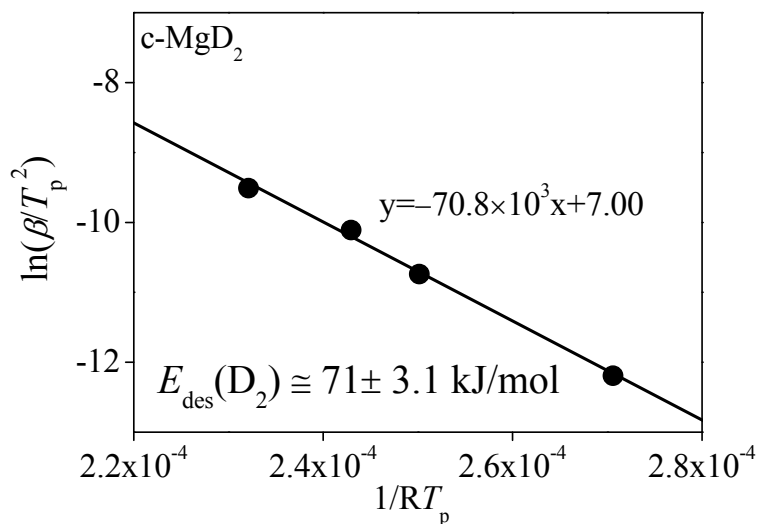
Figure 4-2-22 Kissinger plots on the peak temperature of hydrogen desorption profiles and heating rate for MgD_2 catalyzed with Nb_2O_5.

4.2.4 Characterization of Nb$_2$O$_5$ catalyst

The catalytic effect of Nb$_2$O$_5$ has been discussed in terms of the thermodynamics and kinetics for the reactions in above sections. In this section, characterization of the Nb$_2$O$_5$ is carried out in terms of its chemical state, and the catalytic mechanism is discussed. In order to examine the chemical state of Nb, X-ray absorption fine structure (XAFS) of K-edge for Nb has been investigated by the X-ray absorption spectroscopy (XAS) measurement. The variations of the local atomic coordination around Nb atom are examined by the Fourier transformation of spectra in EXAFS region.

The X-ray absorption near-edge structure (XANES) spectra of the as-milled, dehydrogenated, and hydrogenated samples are shown in Fig. 4-2-23. There are obvious differences among the three references, which are Nb, NbO, and Nb$_2$O$_5$, on the XANES profiles, suggesting that the chemical states of them are totally different. All the spectra obtained from the three samples are very similar, and moreover, the spectra are well corresponded with that of NbO. This variation of chemical state suggests that the Nb$_2$O$_5$ is changed to NbO during the milling process, in other words, Nb^{5+} in Nb$_2$O$_5$ is reduced to Nb^{2+} in NbO. This result is slightly different from previous report by Friedrichs *et al*., where the chemical state of Nb$_2$O$_5$ after ball milling with MgH$_2$ was found to be changed to that of NbO$_2$ as the average state containing Nb$_2$O$_5$ and NbO [14]. Additionally, it is noticed that the spectrum of the dehydrogenated sample is slightly shifted to lower energy position than that of the as-milled sample, and the opposite variation is shown in the spectrum of the hydrogenated sample.

In order to investigate the variation for the chemical state of Nb in detail, in-situ energy-dispersive XAS measurements are performed during both reactions. The white X-ray is used as the incident ray and spectrum can be obtained at shorter time than

conventional measurement system. Additionally, we designed an original environmental cell, in which the inside atmosphere can be controlled. These devices allow to investigate the dynamic variation of the catalyst during the hydrogen absorption and desorption processes. The XANES spectra obtained during in situ hydrogenation reaction in the energy region from 18989 to 18994 eV are shown in Fig. 4-2-24, and the whole spectra are shown in the inset. During the hydrogenation, the XANES spectra have been gradually shifted up to higher energy while, the hydrogen desorption reaction shows the opposite movement as the gradual shift to lower energy position shown in Fig. 4-2-25. These results are different from the results obtained by Friedrichs *et al*., which shows faster variation than our results on the hydrogenation process [14]. The slight shifts of spectra are able to be understood as the slight variation of molecular field around Nb rather than the valence fluctuation of Nb, because the energy shift was smaller than the shift attributed to the valence change (phase changes) of Nb as shown in Fig. 4-2-23. These results indicate that the interaction between hydrogen and NbO is different from that of conventional metal catalysts. For the metal catalysts, the catalytic mechanism is understood as the effect to dissociate hydrogen molecules, and the dissociated hydrogen atoms are overflowed on the metal surface. In this case, it is expected that the XANES profile is unaffected by the hydrogen because the interaction with hydrogen is only on the surface. Therefore, it is expected that the catalytic mechanism of NbO is totally different from the conventional one.

The radial distribution functions obtained by the Fourier transformation of spectra in EXAFS region are shown in Fig. 4-2-26 and 4-2-27. Here, the peak position and the peak area basically correspond to the bond length and coordination number, respectively. The peak observed from 1.5 to 2.0 Å is attributed to the nearest neighbor

atom of Nb, which is corresponded to O atom in NbO. The peak observed from 2.5 to 3.0 Å is assigned to the neighbor Nb atom. Regarding the variation during the hydrogenation reaction, the intensity of the second peak is gradually decreased, although the intensity of the first peak is not changed as shown in Fig. 4-2-26. These results indicate that the structural periodicity between Nb and neighbor Nb is decreased, in other words, the crystalline size is reduced during the catalytic reaction. In the case of the reaction between hydrogen and alloys, it is known that the crystalline size of alloys are decreased by the hydrogen absorption because the metal lattice is expanded and broken by the penetration of hydrogen as mentioned in the section 1.3.1. However, NbO does not absorb hydrogen to form stable hydride phase differently from the hydrogen storage alloys, suggesting that the hydrogen affected to smaller area than that of the alloys. Thus, in the case of large crystal gains, the reduction of crystalline size would be difficult to be observed in radial distribution functions. However, the crystalline size of NbO in Mg is less than 10 nm [21], thereby the small structural variation can be detectable. Therefore, the phenomena shown Fig. 4-2-26 indicate that the crystalline size of NbO is decreased by penetration of hydrogen atoms into NbO crystal.

On the other hand, the radial distribution functions of dehydrogenation reactions are shown in Fig. 4-2-27. There is not a unidirectional tendency as shown in Fig. 4-2-26. In order to decompose of MgH_2, it is necessary to increase temperature thermodynamically, suggesting that the crystalline size is growing up by thermal effect as mentioned in the section 4.2.1. Simultaneously, the hydrogen atoms would penetrate into NbO crystal during the hydrogen desorption process as well. Thus, the Nb-O correlation has no tendency in this process by competition between the above both

phenomena. However, clear increase in the peak intensity corresponding to the Nb-Nb was found after dehydrogenation. When the hydrogen desorption from MgH_2 is completed during the longer reaction time, the hydrogen effect should be lost. After that, the crystalline size is increased by thermal effects.

From above results, the catalytic state and mechanism of Nb oxide is summarized as follows. The redox reaction between Mg and Nb_2O_5 has been observed during ball milling as shown in the result of XANES profile shown in Fig. 4-2-23 and the XRD profile in Fig. 4-2-4, which indicates the growth of MgO phase as shown by the peak at around 42 °. Here, it is possible that MgO has an ability to progress the milling effect for MgH_2 and improves the kinetics of hydrogen absorption and desorption reaction as reported before [22]. As a result, the decreased crystalline size, some defect structures, and the highly dispersed state of the catalyst are obtained. Thus, the reduction of Nb_2O_5 to NbO with MgO formation, which supports the better dispersion state of NbO, is important process to realize remarkable catalytic effect. Furthermore, the catalytic mechanism of NbO is different from the conventional metal catalysts. NbO dissociates H_2 molecule, and then the generated hydrogen atoms diffuse and pass through NbO crystal, and hydrogen atoms are immediately transferred from NbO to Mg because of the weakly affinity between hydrogen and NbO.
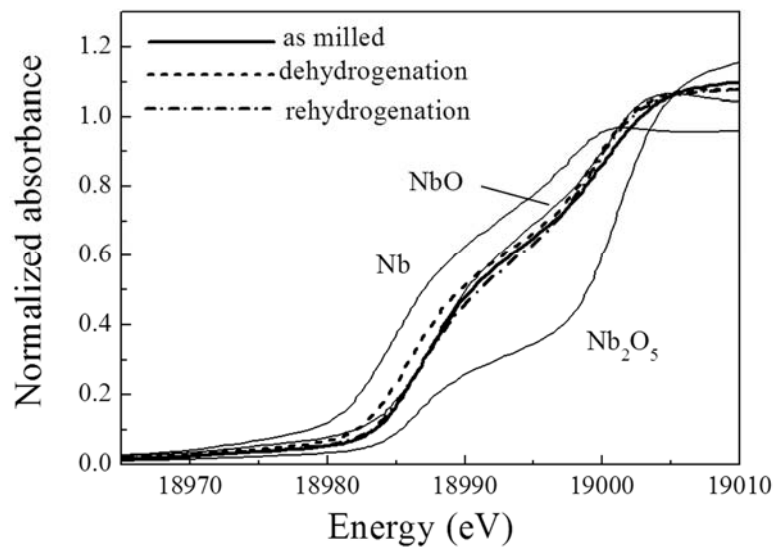
Figure 4-2-23 XANES spectra of the samples after the milling, dehydrogenation, and rehydrogenation. XANES spectra of Nb, NbO, and Nb_2O_5 are also shown as references.
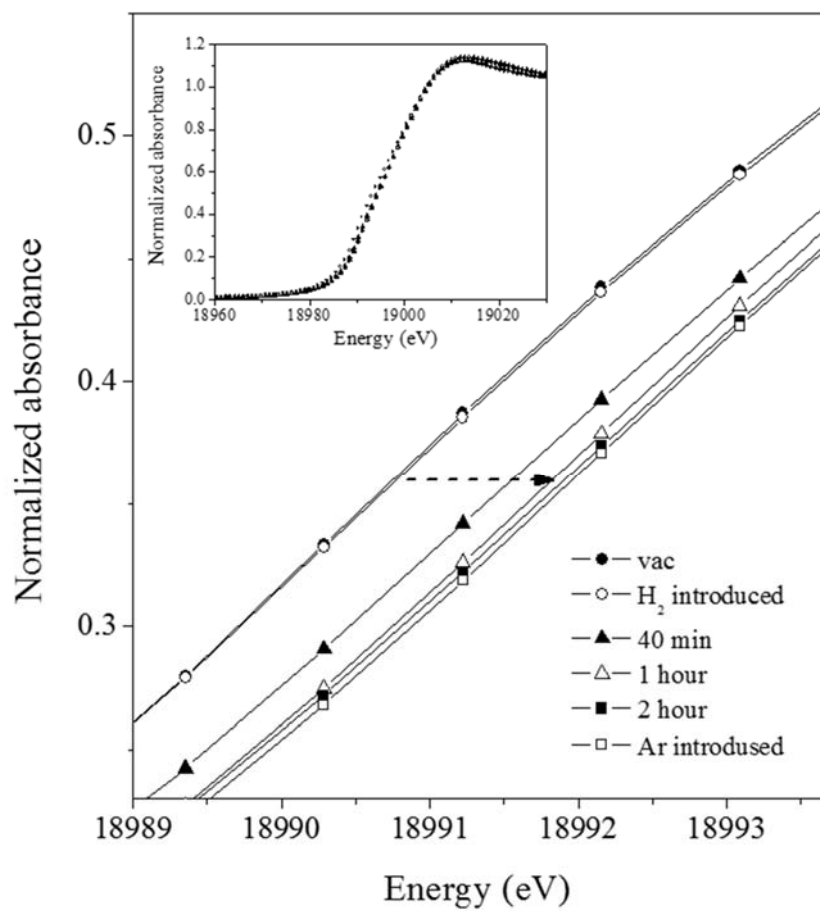
Figure 4-2-24 In situ XANES spectra during the hydrogenation reaction of the Mg catalyzed with Nb_2O_5 at room temperature.
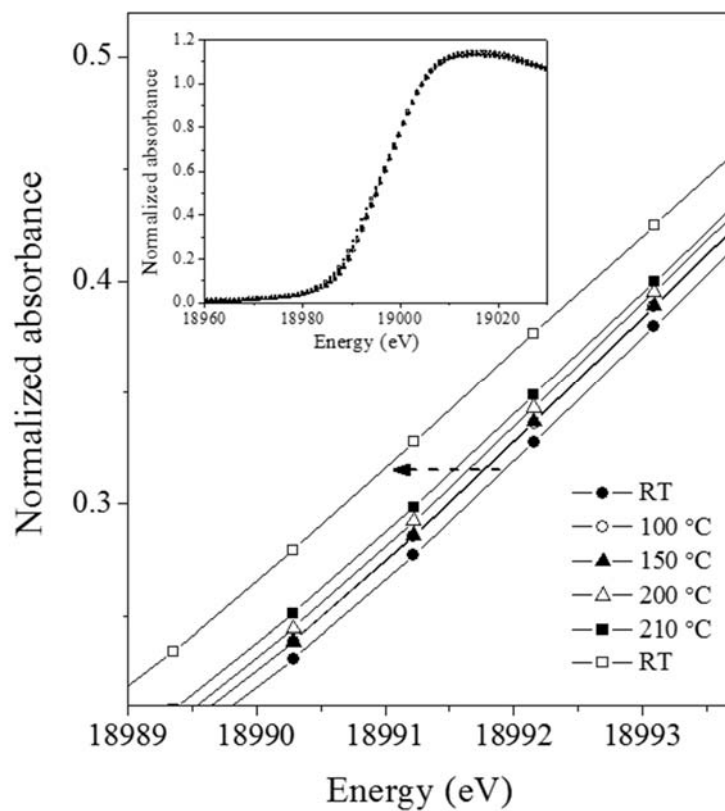
Figure 4-2-25 In situ XANES spectra during the dehydrogenation reaction of the MgH$_2$ catalyzed with Nb$_2$O$_5$ under Ar flow condition.
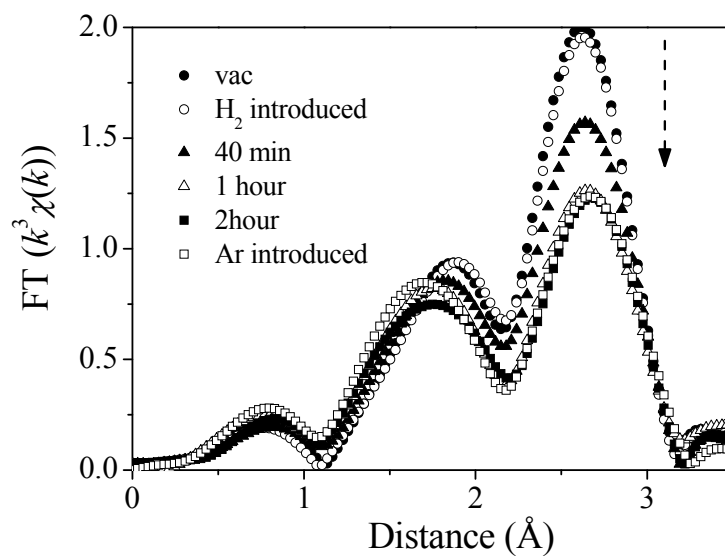
Figure 4-2-26 Radial distribution functions obtained by the Fourier transformation of the EXAFS regions measured during the hydrogenated reaction of the Mg catalyzed with Nb$_2$O$_5$ at room temperature.
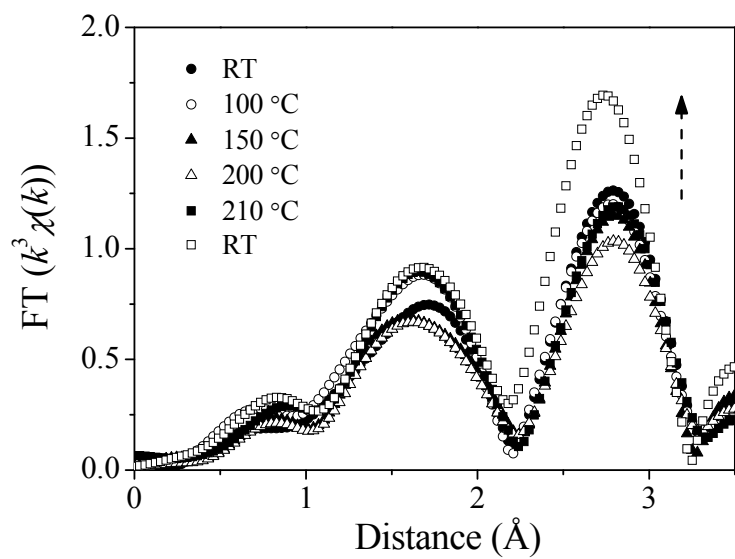
Figure 4-2-27 Radial distribution functions obtained by the Fourier transformation of the EXAFS regions measured during the dehydrogenated reaction of the MgH_2 catalyzed with Nb_2O_5 under Ar flow condition.

References

[1]   G. Barkhordarian, T. Klassen and R. Bormann: *Scr. Mater.* 49 (2003) 213-217.

[2]   N. Hanada, T. Ichikawa, S. Hino and H. Fujii: *J. Alloys Compd.* 420 (2006) 46-49.

[3]   J. Huot, I. Swainson and R. Schulz: *Annales de Chimie: Science des Materiaux.* 31 (2006) 135-144.

[4]   N. Hanada, T. Ichikawa, S. Isobe, T. Nakagawa, K. Tokoyoda, T. Honma, H. Fujii and Y. Kojima: *J. Phy. C.* 113 (2009) 13450-13455.

[5]   N. Hanada, T. Ichikawa and H. Fujii: *Physica B: Condensed Matter.* 383 (2006) 49-50.

[6]   Y. Fukai, *The Metal-Hydrogen System.* 1993, Springer-Verlag.

[7]   H. J. G. J. Renner: *Z. Metallkde.* 69 (1978) 639-642.

[8]   R. K. Singh, T. Sadhasivam, G. I. Sheeja, P. Singh and O. N. Srivastava: *Int. J. Hydrogen Energy.* 38 (2013) 6221-6225.

[9]   A. Denis, E. Sellier, C. Aymonier and J. L. Bobet: *J. Alloys Compd.* 476 (2009) 152-159.

[10] Y. Kojima, Y. Kawai and T. Haga: *J. Alloys Compd.* 424 (2006) 294-298.

[11] X. B. Yu, Y. H. Guo, H. Yang, Z. Wu, D. M. Grant and G. S. Walker: *J. Phys. Chem. C.* 113 (2009) 5324-5328.

[12] J. F. Fernández and C. R. Sánchez *J. Alloys Compd.* 340 (2002) 189-198.

[13] N. Hanada, T. Ichikawa and H. Fujii: *J. Alloys Compd.* 446-447 (2007) 67-71.

[14] O. Friedrichs, D. Martínez-Martínez, G. Guilera, J. C. S. López and A. Fernández: *J. Phys. Chem. C.* 111 (2007) 10700-10706.

[15] F. Leardini, J. R. Ares, J. F. Fernández, J. Bodega and C. Sánchez: *Int. J. Hydrogen Energy.* 36 (2011) 8351-8357.

[16] J. Huot, G. Liang, S. Boily, A. Van Neste and R. Schulz: *J. Alloys Compd.* 293-295 (1999) 495-500.

[17] S. Naito, M. Yamamoto, T. Miyoshi, M. Mabuchi, M. Doi and M. Kimura: *J. Chem. Soc., Faraday Trans.* 92 (1996) 3407-3410.

[18] H. Hagi and Y. Hayashi: *Transactions of the Japan institute of metals.* 28 (1987) 368-374.

[19] T. Maeda, S. Naito, M. Yamamoto, M. Mabuchi and T. Hashino: *J. Chem. Soc., Faraday Trans.* 89 (1993) 4375-4379.

[20] C. H. Mak, J. L. Brand, B. G. Koehler and S. M. George: *Surf. Sci.* 188 (1987) 312-320.

[21]   N. Hanada, E. Hirotoshi, T. Ichikawa, E. Akiba and H. Fujii: *J. Alloys Compd.* 450 (2008) 395-399.

[22]   K. F. Aguey-Zinsou, J. R. Ares Fernandez, T. Klassen and R. Bormann: *Mater. Res. Bull.* 41 (2006) 1118-1126.

5.   Conclusion

In order to characterize the catalytic effects of transition metal oxides, ZrO_2 and Nb_2O_5, the properties of hydrogen absorption and desorption reactions have been accurately investigated from the kinetic and thermodynamic points of view by using various experimental techniques. Particularly, the variation of the chemical state of Nb_2O_5, which is the most effective catalyst, during hydrogenation and dehydrogenation reactions has been investigated in-situ. The results obtained in this thesis are summarized as follows:

1.   The catalytic effect of ZrO_2 for the reaction between hydrogen and Mg has been investigated as shown in the chapter 4.1. For the hydrogen desorption reaction of MgH_2, the reaction rate for decomposition of MgH_2 catalyzed with ZrO_2 is clearly faster than that of MgH_2 without catalyst, and the reaction rate is affected by the amount of ZrO_2. For the hydrogen absorption reaction of Mg, the hydrogen absorption rate of Mg is improved by the catalysis of ZrO_2, resulting in the hydrogen absorption even at room temperature. Additionally, it has been found that the ball milling with ZrO_2 affects MgH_2 not only to change its structure but also to add ZrO_2 as the catalyst.

2.   The catalytic effect of Nb_2O_5 for dehydrogenated reaction of MgH_2 has been investigated and the results are discussed in section 4.2.1. The reaction rate of dehydrogenation reaction is found to be improved clearly by addition of Nb_2O_5. The crystalline size of MgH_2 is an important factor for the kinetics of decomposition of MgH_2. The crystalline growth of MgH_2 can be prevented by performing the hydrogenation at low temperature condition. In addition, the hydrogenation and rehydrogenation treatment

further improve the kinetics, indicating that the dispersed Nb_2O_5 is changed to more homogeneous and active state as catalyst during the hydrogen absorption and desorption processes. The activation energy of hydrogen desorption reaction for MgH_2 with and without Nb_2O_5 are estimated as 70 kJ/mol and 129 kJ/mol, respectively, indicating that the addition of Nb_2O_5 decreases the surface barrier, which is attributed to recombination of hydrogen molecule.

3.	The catalytic effect of Nb_2O_5 for hydrogenation reaction of Mg has been accurately investigated as discussed in section 4.2.1. In order to prevent the influence of the reaction heat and understand the essential kinetic properties, the reactions are performed under low temperature below 0 °C and 0.2 MPa of hydrogen pressure conditions. It is noteworthy that the Mg catalyzed with Nb_2O_5 can absorb hydrogen even at −50 °C, which is the lowest value as reported so far. The activation energy of hydrogen absorption reactions for Mg with and without Nb_2O_5 are found to be 38 kJ/mol and 61 kJ/mol, respectively. Thus, it is clarified the reaction rate for hydrogenation reaction of Mg has been improved drastically by the addition of Nb_2O_5, and it is suggested that the determining step of hydrogen absorption is changed from the surface reaction to hydrogen diffusion process.

4.	The thermodynamic properties of the Mg with and without Nb_2O_5 for hydrogen storage have been investigated in the section 4.2.2. For the non-catalyzed Mg, its hydrogen capacity is estimated about 7.1 wt%, and the enthalpy and entropy changes attributed to the reaction between hydrogen and Mg are estimated to be 77 kJ/mol H_2 and 138 J/mol K, respectively. On the other hand, the hydrogen capacity of the Mg catalyzed

with Nb_2O_5 is estimated about 6.3 wt%, and the enthalpy and entropy changes are estimated 75 kJ/mol H_2 and 136 J/mol K, respectively. The difference of hydrogen capacity is corresponding to the weight of Nb_2O_5 added as catalyst. The thermodynamics properties of Mg have not been changed by addition of Nb_2O_5. It is confirmed that the ball milling and addition of Nb_2O_5 have no significant effect for the thermodynamic properties.

5.   In order to clarify the rate-determining step of hydrogen absorption and desorption reactions for c-Mg, the kinetics properties of c-Mg have been investigated by using deuterium instead of hydrogen as shown in the section 4.2.3. The activation energy of deuterium absorption and desorption reactions for Mg catalyzed with Nb_2O_5 are estimated to be 41 kJ/mol and 71 kJ/mol, respectively. These values have no significant isotopic effects, while the reaction rates of both H and D systems are different. Thus, it is difficult to discuss the kinetic difference between both systems from the analysis in this work.

6.   In order to define the interaction between Mg and Nb_2O_5, the variation of the structure of Mg and the chemical states of Nb_2O_5 have been investigated by XRD and XAS measurements, respectively, as discussed in the sections 4.2.1 and 4.2.4. Regarding Mg, the ball milling leads a part of MgH_2 to change MgO, and the crystalline size of MgH_2 is strongly affected by temperature condition of the rehydrogenation treatment. As a result, Nb_2O_5 is effectively reduced to NbO by the ball milling with MgH_2. By the in-situ XAS measurements, the gradual and slight variations of the chemical state of Nb during hydrogenation and dehydrogenation reactions of Mg are observed. The XAS

results indicated that the hydrogen is dissociated by the interaction with NbO and is diffused through NbO, indicating that the catalytic mechanism of oxides is different from that of transition metal catalysts.

The catalytic effect of Nb_2O_5 drastically improves the reaction rates of the hydrogen absorption and desorption reactions of Mg although the thermodynamic parameters such as enthalpy and entropy changes of Mg are not changed. Considering the experimental results, the catalytic mechanism of Nb_2O_5 can be understood as follows:

1. The redox reaction between MgH_2 and Nb_2O_5 occurs to form MgO and NbO, which is catalytic active state for the dissociation of H_2.

2. NbO possesses peculiar catalytic effects differently from that of metal catalysts. It is expected that the dissociated hydrogen by NbO diffuse and pass through NbO.